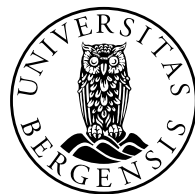Master's thesis in physical oceanography

The structure and transport of the western branch of the Norwegian Atlantic Current using stream-coordinates on Seaglider data

Håvard Vindenes
June 2013

Geophysical Institute
University of Bergen

Acknowledgements

Abstract

Data from 8 Seaglider transects, obtained along the Svinøy section in the Norwegian Sea during a 7-month period between May and December of 2012, have been used to test the applicability of stream-coordinate averaging on the Norwegian Atlantic Front Current, an unstable, meandering, baroclinic frontal jet. Additionally, we have estimated the transport of Atlantic Water in the western branch of the Norwegian Atlantic Current from absolute geostrophic velocity estimates.

The Seaglider is an unmanned underwater vehicle, capable of dives down to a depth of 1000 m. It collects hydrographic data, and estimates a depth-averaged current for each dive which allows for an estimate of absolute geostrophic velocity and thus the geostrophic velocity at maximum dive depth.

The stream-coordinate average of the Norwegian Atlantic Front Current is narrower and stronger than the corresponding Eularian average, with a current core 40 km wide and with maximum speed exceeding 30 cm/s, bearing a stronger resemblance to the current core observed in individual transects. The Eularian average, in contrast, results in a current more than 80 km wide with a maximum speed of approximately 18 cm/s.

Transport estimates from the western branch of the Norwegian Atlantic Current are sparse relative to the eastern branch, and previous estimates based on dynamic calculations from hydrography have been reliant on an assumption of no motion at mid-depth. Our transport estimates of Atlantic water (defined as water with salinity greater than 35) in the western branch of the Norwegian Atlantic Current show an average value of 4.7 Sv (1 Sv = 10^6 m^3/s). The average contribution of the barotropic component of the transport is 2.6 Sv, which is equal to 54 % of the total transport. A comparison between the estimated current at 1000 m depth, derived from the Seaglider data, and measurements from a moored current-meter has been made in order to verify the validity of our current- and transport estimates.

Contents

Chapter 1

Introduction

The Norwegian Atlantic Current (NwAC) is an extension of the North Atlantic Current which stretches into the Norwegian Sea and ultimately into the Arctic Ocean via the Fram Strait and the Barents Sea. The eastward flowing North Atlantic Current splits into two northward flowing branches, one of which enters the Rockall Trough while the other flows through the Iceland Basin toward Iceland. The two major pathways where the Atlantic water (AW) enters the Nordic Seas are through the Faroe-Shetland Channel and over the Iceland-Faroe Ridge on the southwest border of the Norwegian Sea. The NwAC continues into the Norwegian Sea as a two-branch system. The eastern branch, called the Norewgian Atlantic Shelf Current (NwASC), travels northward along the Norwegian Continental Shelf as a nearly barotropic shelf edge current, while the western branch, called the Norwegian Atlantic Front Current (NwAFC), originates in the Iceland-Faroe Front and continues as a baroclinic frontal jet in the Polar Front guided by dominant topographic features all the way to the Fram Strait (Orvik and Niiler, 2002; Poulain et al., 1996). Figure 1.1 shows the geography of the Norwegian Sea and it's surroundings as well as an illustration of the major pathways of near-surface flow of AW as derived by drifter data by Orvik and Niiler (2002).

The Svinøy section, located approximately 500 km downstream from the Iceland-Scotland Ridge, stretches northwestward from the edge of the Norwegian Continental Shelf toward the interor of the Norwegian Basin (See location in figure 1.3). The width of the NwAC in this area is relatively narrow, typically 200 - 250 km wide. Water masses in the section, and in the Nordic Seas in general are mostly composed of water of Arctic and Atlantic origin (See TS-diagram for the main Nordic Seas water masses in figure 1.2). AW in the Nordic Seas is commonly defined as water masses with salinity greater than 35. Norwegian Sea Deep Water (NSDW), a result of the mixing of AW and the colder and fresher Polar water, typically has salinities of around 34.9 and temperatures below 0 °C and originates in the Greenland Gyre and the Arctic Ocean (Aagaard et al., 1985). In addition to water of Atlantic and Arctic origin, the Norwegian Coastal
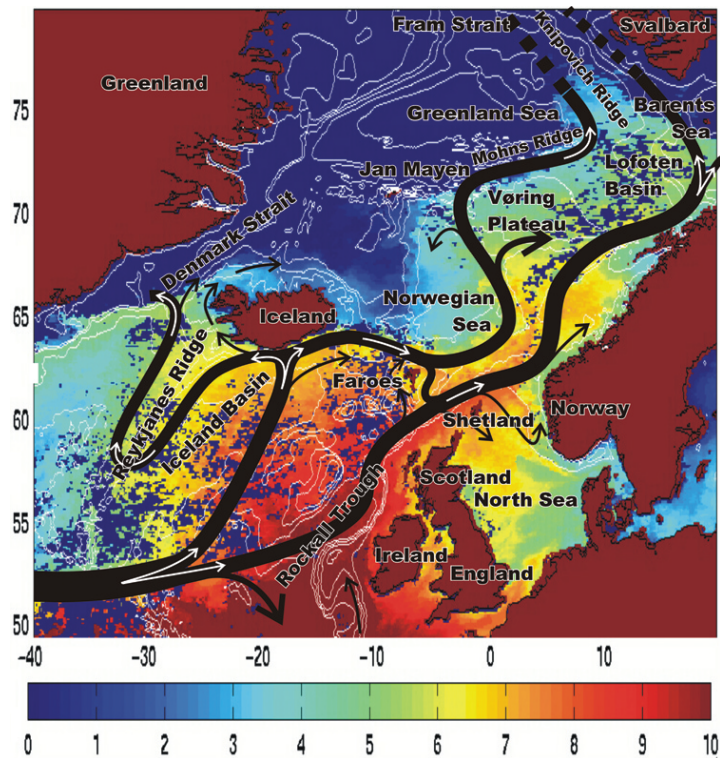
Figure 1.1: Major pathways of the near-surface flow of Atlantic water in the Nordic Seas and the North Atlantic (black arrows) derived from near-surface drifter data over sea surface temperature ($°C$). Figure aquired from Orvik and Niiler (2002).

Current, located on the eastern side of the Norwegian Sea on the Norwegian continental shelf, is a source of relatively fresh Norwegian Coastal Water (NCW). It originates in the Baltic Sea and gathers freshwater runoff along the coast of Norway (Mork, 1981). Salinity in the coastal current increases when it encounters AW in the North Sea and Norwegian Sea and mixes on the way north. Typically water in coastal areas with salinities below 35 is considered coastal water (Sætre and Ljøen, 1972).

The Svinøy section has been monitored for more than half a decade by the Norwegian Institue of Marine Research, using traditional hydrographic methodology. Since 1995 the Geophysical Institue at the University of Bergen has monitored the same area using moored current meters (Orvik et al., 2013). The current meter moorings cover the eastern branch of the NwAC to a greater extent than the western branch. Thus, transport estimates from the NwAFC are comparatively sparse, and have typically been based on dynamic calculations from hydrography.
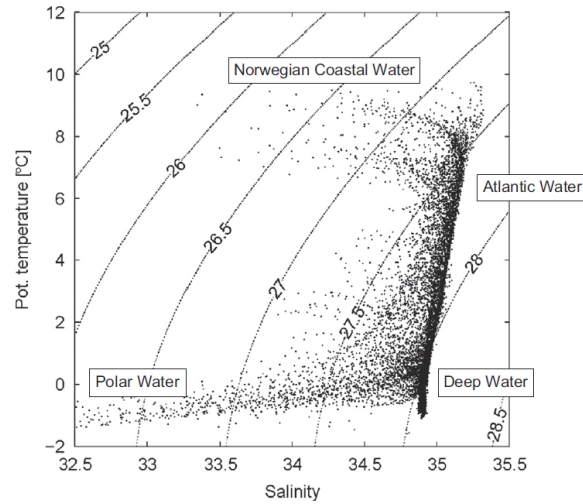
Figure 1.2: Temperature-salinity diagram displaying the main water masses found in the Nordic Seas. Figure aquired from Høydalsvik et al. (2013).

Due to the unstable nature of the NwAFC, the current meanders and the core shifts laterally along the Svinøy section, but historically it has been observed most frequently in the vicinity of the 2000m isobath (Orvik et al., 2001; Høydalsvik et al., 2013). Orvik et al. (2001) describe it as a 30 - 50 km wide 400 m deep jet with maximum speed of 87 cm/s. In a study using Seaglider data, Høydalsvik et al. (2013) described the core of the NwAFC, after applying Eularian temporal averaging on 9 transects, as a 50 km wide and 400 m deep current. They found it to be centered between the 1500 and 2000 m isobath, with maximum speeds of around 20 cm/s. The relatively low maximum speed found by Høydalsvik et al. (2013) is a result of the Eularian averaging and the subsequent smoothing of the hydrographic profiles and hence the velocity profile, while the max speed presented by Orvik et al. (2001) was measured directly by shipmounted ADCP. The current core in the eastern branch of the NwAC does not shift laterally as much as in the western branch and is typically centered over the 500m isobath. Orvik et al. (2001) describe the NwASC in the Svinøy section as a 40 km wide, topographically trapped current filling the water column between the 700 and 200m isobath, with an annual mean velocity of 30 cm/s. The core is observed to have a barotropic structure. The area between the two branches of the NwAC is filled with AW as a result of exchange of water between them (Rossby et al., 2009).
The Atlantic inflow and hence the NwAC has shown evidence of seasonality as the magnitude of the inflow, historically, has been strongest during winter (Orvik et al., 2001; Mork and Skagseth, 2010; Mork and Blindheim, 2000). The seasonality in both branches of the NwAC can be linked to seasonal variation in wind forcing (Orvik and Skagseth, 2003; Voet et al., 2010).
Transport estimates of the NwAC in the Svinøy section vary substantially depending on
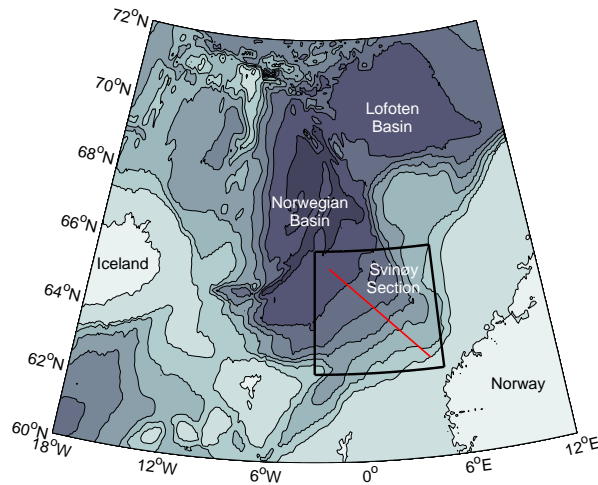
Figure 1.3: Bathymetry map of the Norwegian Sea and the surrounding areas with a contour interval of 500 m. The Svinøy section is marked by a red line. The black frame around the Svinøy section marks the area covered in figure 4.3 and 5.3. The Bathymetry database was aquired from National Geophysical Data Center (1995).

the method used to measure or calculate the velocity fields. Orvik et al. (2001) estimated a mean baroclinic transport of 3.4 Sv in the western branch, which in addition to the 4.2 Sv transport measured in the eastern branch adds up to a total of 7.6 Sv. Østerhus et al. (2005) found the average Atlantic Inflow both over the Iceland-Faroe Ridge and through the Faroe-Shetland Channel to be 3.8 Sv, which yields the same total transport of 7.6 Sv. Mork and Blindheim (2000), considering water warmer than 1°C, estimated the mean baroclinic transport in the western branch to be 4.1 Sv during winter and 2.5 Sv and 3.7 Sv during the spring and summer months, respectively. A substantially lower total transport of 1.7 Sv, based on dynamic topography, was estimated by Mork and Skagseth (2010). Høydalsvik et al. (2013), using Seaglider data which includes depth-averaged current and hence the opportunity to estimate total geostrophic velocity, found a mean transport of 6.8 Sv in the NwAFC (3.2 Sv of which was due to the baroclinic component). They concluded that with their results from the transport of AW in the western branch showing more than 50 % contribution from the barotropic component, it is likely that use of a level of no motion in this area will lead to significant underestimates of the total transport.

The data used in this study, was obtained during a 7 month Seaglider survey in the Svinøy section from May to December of 2012. This was one of the first glider surveys performed as part of The Norwegian Atlantic Current Observatory (NACO) program, which was initiated in 2012. NACO is a monitoring program of the NwAC in the Svinøy section as well as sections in the Lofoten Basin. The project was funded by the Norwegian Research Council, and is hosted by the Geophysical Institute at the University of

Bergen.

The Seaglider that obtained the data used in this study (SG560) was deployed on the 23rd of May, and made 8 transects back and forth along the Svinøy section, from the Norwegian continental shelf edge at 62.82°N, 4.25°E to the interior of the Norwegian Basin at 65.50°N, 2.00°W (illustrated by the red line in figure 1.3), being retrieved on the 20th of December. The Seaglider was deployed seaward of the core of the NwASC to avoid being carried downstream by the strong shelf edge current. In an area like this where the flow in the whole water column is relatively fast, compared to the 25 cm/s speed of the Seaglider, the Seaglider will not be able to stay on track. Therefore the study focuses on the Western Branch of the NwAC. Most dives are approximately 1000 m deep as long as the bottom topography allows it. This is more than deep enough to cover the portion of the water column which is occupied by AW, which typically does not extend deeper than 600 m in the Svinøy section.

This study builds on the methods and instrumentation utilized by Høydalsvik et al. (2013), and is a continuation of the monitoring of the inflow of AW into the Nordic Seas with special focus on the western branch of the NwAC. We wish to utilize the strengths of the Seaglider and the data it obtains, and to apply methods that take advantage of it. Stream-coordinate averaging is a method that has been applied in the Gulf Stream to accurately portray the average state of the current core of a baroclinic jet (Bower and Hogg, 1996; Halkin and Rossby, 1985; Johns et al., 1995). Using stream-coordinate averaging instead of the traditional Eularian averaging, we aim to remove the smoothing effects which can be expected when using typical Eularian averaging on a meandering and unstable jet. Thus, we hope to produce a more accurate rendition of the average state of the NwAFC than that presented by Høydalsvik et al. (2013). Also we wish to investigate the mid-depth flow in the section, and to which degree it influences the volume transport of AW northward into the Norwegian Sea.

The study is structured as follows; A theoretic description of a few key concepts related to dynamical processes and stream-coordinate averaging are presented in Chapter 2. Chapter 3 is a description of the instrumentation and the data-processing. Next, the results are presented in Chapter 4. Central findings will be presented and discussed in in Chapter 5. Finally, concludinge remarks are made in Chapter 6.

Chapter 2

Theory

2.1 Geostrophic Current

When studying large scale motions in the ocean, one has to account for the effect of the Earth's rotation on the system. The apparent deflection of objects moving over the surface of the Earth, without being frictionally bound to it, is called the Coriolis effect. A current is in geostrophic equilibrium when the horizontal pressure gradient force is balanced by the Coriolis force. The equations for geostrophic balance are derived from the momentum equations by assuming the acceleration term is dominated by the Coriolis acceleration and that friction is negligable. The Rossby number is a dimentionless number that defines the ratio of inertial force to the Coriolis force:

$$R_o = \frac{U}{fL} \tag{2.1}$$

U is the velocity scale, $f = 2\Omega \sin \varphi$ is the Coriolis parameter, Ω is the rotation rate of the Earth, φ is latitude, and L is the horizontal length scale. If the Rossby number is sufficiently small, meaning much less than one, geostrophic equilibrium should be approximately satisfied, and motion can be described by

$$f\hat{\mathbf{k}} \times \mathbf{u} = -\frac{1}{\rho}\nabla p - g\hat{\mathbf{k}} \tag{2.2}$$

where $\hat{\mathbf{k}}$ is the unit vector in the upward direction, $\mathbf{u} = (u, v, w)$ is the velocity vector, ρ is density, $\nabla = (\frac{\partial}{\partial x}, \frac{\partial}{\partial y}, \frac{\partial}{\partial z})$ is the gradient operator, p is pressure, and g is the gravity acceleration. The horizontal momentum equations become:

$$-fv = -\frac{1}{\rho}\frac{\partial \rho}{\partial x} \tag{2.3a}$$

$$fu = -\frac{1}{\rho}\frac{\partial \rho}{\partial y} \tag{2.3b}$$

2.2 Thermal wind

Geostrophic motion may arise during an adjustment to horizontal density gradients and keep a stratified fluid from gravitational equilibrium (Cushman-Roisin and Beckers, 2011). The thermal wind relation was first used in meteorology do describe the connection between the vertical shear of geostrophic winds and horizontal temperature gradients in the atmosphere. The vertical shear of the geostrophic wind between any two isobaric surfaces is related to the horizontal gradient of the thickness of the layer (Wallace and Hobbs, 2006). Figure 2.1 illustrates the thermal wind relation, and the connection between the layer thickness and temperature.
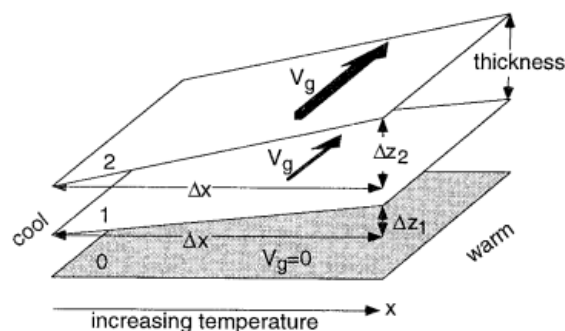

Figure 2.1: Illustration of a baroclinic example of the thermal wind relation. Three isobaric surfaces, starting from a horizontal surface level of no geostrophic motion (surface 0) experience increasing tilt with decreasing pressure. Density decreases with x as the cool air is denser than warm air. The increasing tilt results in a positive vertical shear of the geostrophic velocity V_g. Figure aquired from Stull (1999).

In order to calculate the cross track baroclinic velocities and volume transport in the Svinøy section we have utilized the thermal wind equation (equation 2.4) expressed as a relation between the horizontal density gradient and the vertical velocity shear:

$$\frac{\partial v}{\partial z} = -\frac{g}{\rho_0 f}\frac{\partial \rho}{\partial x} \tag{2.4}$$

v is the velocity perpendicular to the transect, z is the vertical coordinate (positive upward), x is the along-track coordinate, g is the acceleration of gravity, and ρ_0 is the reference density (from Bousinessq approximation).
In our calculations we have used a layered system (equation 2.5) to calculate the velocity

difference between two depths. Starting from the deepest measurements ($z = -H$), assuming a reference velocity $v(-H) = 0$, and calulating the velocity for each bin up to the surface.

$$\frac{\Delta v}{\Delta z} = -\frac{g}{\rho_0 f}\frac{\Delta \rho}{\Delta x} \tag{2.5}$$

We define $\Delta v = v_1 - v_2$ and $\Delta \rho = \rho_2 - \rho_1$, where v_1 is the velocity in the layer above v_2, and ρ_1 and ρ_2 are the densities of two neighbouring stations along the x-axis (ρ_2 represents the station further along the x-axis), at the same depth as v_1. In our case, calculations were made using 1m vertical bins, and thus $\Delta z = 1$. This leaves us with

$$v_1 = v_2 - \frac{g}{\rho_0 f}\frac{\rho_2 - \rho_1}{\Delta x} \tag{2.6}$$

which, when integrated from the deepest bin up to the surface, assuming no motion at $z = -H$, provides the baroclinic component of the current at all intermediate depths:

$$v_{baroclinic}(z) = -\frac{g}{\rho_0 f}\int_{-H}^{z}\frac{\partial \rho}{\partial x}dz \tag{2.7}$$

2.3   Barotropic, baroclinic and absolute velocity

Absolute geostrophic velocity is the sum of a baroclinic- and barotropic component (See figure 2.2). Baroclinic conditions are characterized by pressure- and density surfaces being inclined to one another. Baroclinic velocity varies with depth and is a result of the horizontal density shear. Fast surface currents are mostly found in regions of strong baroclinicity. Barotropic conditions are found in well mixed surface water as well as in the deep ocean below the permanent thermocline where density and pressure surfaces are virtually functions of depth, and the isopycnal and isobaric surfaces are parallel (Brown et al., 2001). The barotropic component is independent of depth. Calculating velocity estimates from hydrographic data has typically been reliant on the assumption of a reference level of no motion. The "level of no motion" assumption is built on the idea that at a fairly deep level where the horizontal pressure gradient force is zero, and the geostrophic velocity therefore also is zero. However, a barotropic component may contribute to the current beyond the reference level. We have applied the same equations as those described by Høydalsvik et al. (2013) in order to calculate geostrophic velocity. The absolute geostrophic velocity at any given depth z can be presented as:

$$v(z) = v(-H) - \frac{g}{\rho_0 f}\int_{-H}^{z}\frac{\partial \rho}{\partial x}dz \tag{2.8}$$
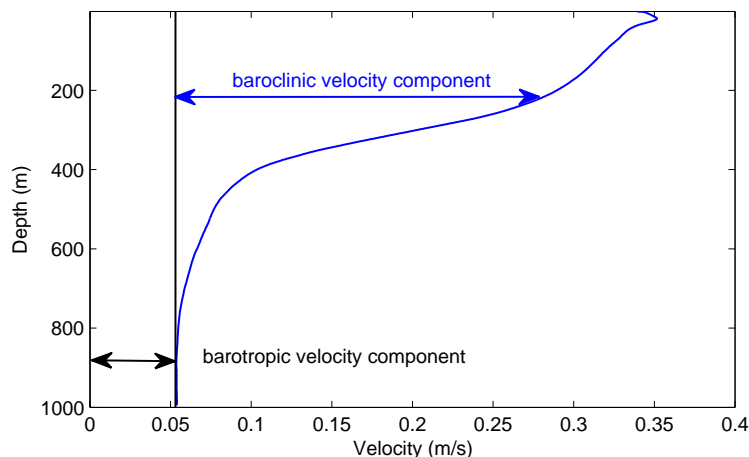
Figure 2.2: Example of a geostrophic current velocity profile.

The depth-averaged velocity V over dive depth H is the veritcal integral of equation 2.8:

$$V = \frac{1}{H} \int_{-H}^{0} v(z) dz \qquad (2.9)$$

The Seaglider provides us with estimates of the depth-averaged flow, thus allowing us to calculate the velocity at maximum depth by subtracting the depth-averaged baroclinic velocity from equation 2.9, which yields:

$$v(-H) = V - \frac{1}{H} \int_{-H}^{0} v_{baroclinic}(z) dz \qquad (2.10)$$

Once the velocity at maximum depth is obtained we can insert $v(-H)$ into equation 2.8 and calculate an estimate for the total geostrophic velocity at any depth.

2.4 Eularian- and stream-coordinates

Stream-coordinates are applied to the data in this study in order to remove the smoothing effects that follow temporal averaging of a meandering current in a Eularian coordinate system. An eularain coordinate system is a typical system in which the properties

of a fluid parcel are assigned to points in space for any given time. An Eularian time average is simply the average state of a certain property in a certain location over time. Therefore when studying a specific feature in the ocean like the core of the NwAFC which shifts laterally along the section for each measured transect, the Eularian averaging will not produce a realistic average state of the current core, but rather an average state of the area in which the core is found. Stream-coordinates is a system where each fluid parcel is located not in a specific position in geographic space, but rather in relation to a specific feature, like the core of the NwAFC. Before applying a temporal average, each transect is shifted so that the origin is aligned with the current core. Thus the resulting average state of the current core in a stream-coordinate system should be affected only by variation in the properties of the core, and not the variation in the geographic position along the section.

The conversion from a typical Eularian coordinate-system to a stream coordinate system varies with what kind of instrumentation has been used. Typically it is a network of moored current meters (Bower and Hogg, 1996; Halkin and Rossby, 1985; Johns et al., 1995), but stream-coordinates are appliccable to CTD-sections as well.

Technically, there are three steps to completing a conversion from a geographic coordinate system to a stream-coordinate system. First, one should locate the centre of the stream for each transect, and adjust the origin accordingly. Next, determine the downstream direction, and finally, the east- and north velocity components transformed into downstream and cross-stream components according to the downstream direction. However, when working with Seaglider data, we have no direct current measurements at given depths, and therefore, defining the downstream direction in the core of the NwAFC is not feasible. The direction of the depth-averaged current (which we can estimate with Seaglider data) will not necessarily be representative for the direction in the core. As a result of this, in this study, the conversion to stream-coordinates only covers step one and three. Each transect has been shifted along the section to line their origins up in accordance with each other, and the depth-averaged current data have been decomposed into along- and cross-track components relative to the section. The origin for every transect has been set to where the 1027.6 kg/m^3 isopycnal crosses 200 m depth, a location found to be representative for the position of the Polar Front and the core of the NwAFC in all transects where these features are distinguisable. The corresponding temperature and salinity values in this location is typically around 6.5°C and 35.15, respectively.

Chapter 3

Data and Methods

3.1 The Seaglider

3.1.1 Vehicle description

The Seaglider is a small unmanned underwater vehicle (UUV), used for oceanographic measurements along a sawtooth pattern from the surface down to a programmed depth, and back to the surface. It was developed at the University of Washington, designed to operate most efficiently on long range missions, operating for several months over thousands of kilometers, and with dives as deep as 1 km (Rudnick et al., 2004). Relative to techniques reliant on instruments on board or operated from research vessels, the Seaglider is highly cost efficient and also provides data of higher resolution in both time and space (Eriksen et al., 2001).

The Seaglider consists of a flooded, streamlined fiberglass fairing, inside which is located an interior aluminium pressure hull. Wings and rudders are attached to the exterior of the fiberglass fairing, and attached to the tail of the main vehicle body is a mast with an Iridium/GPS antenna on the tip (See technical specifications in table 3.1 for details, and figure 3.1 for an illustration of the vehicle and its parts). The pressure hull is designed to have the same compressibility as seawater, which results in about 10% energy savings (iRobot corporation, 2012). A rigid pressure hull would maintain the same volume at all depths, and therefore aquire a positive buoyancy when the surrounding waters increase in density. The isopycnal hull eliminates that increase in buoyancy.

The Seaglider does not rely on a propeller for propulsion. A Variable Buoyancy Device (VBD) adjusts the buoyancy of the Seaglider by pumping oil between a reservoir inside the pressure hull and a external bladder located in the flooded aft fairing. Pumping oil into the bladder increases the volume of the vehicle, but the mass remains the same. Bleeding oil from the bladder back into the reservoir has the oposite effect. The change in buoyancy leads to vertical motion, which is transformed into horizontal
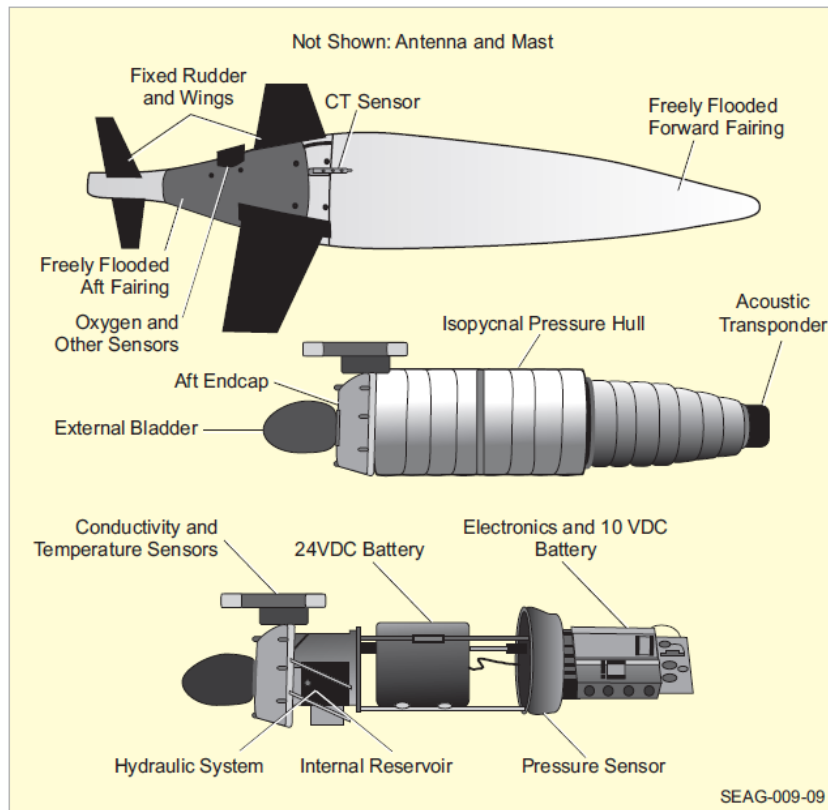
Figure 3.1: The Seaglider and its primary parts (iRobot corporation, 2012).

motion by the Seaglider's wings. The attitude of the Seaglider is controlled by shifting mass (the battery) within the pressure hull. The pitch is controlled by shifting the mass toward the fore or the aft of the hull. Adjustment of the course is accomplished by inducing roll, which results from shifting mass along the Seaglider's lateral axis.

The Seaglider is autonomous during dives, however, it is in contact with the basestation on land every time it surfaces. Once a connection is established via the Iridium satellite phone, the Seaglider transfers data files from the previous dive and receives command files for the next dive. This regular communication allows for frequent input from the pilots who can observe the incoming data and adjust dive parameters for upcoming dives if necessary.

3.1.2 Dive cycle

As described by Eriksen et al. (2001), before the Seaglider starts a dive, it pitches forward so that the nose points down. The VBD pumps to obtain target surface buoyancy so that the antenna is above the surface. The GPS receiver is powered on and obtains a position fix, then the glider initiates contact with the control computer, sends data files

Body size	Length 2 m (+antenna mast length 1m), max diameter 30 cm
Lift surfaces	Wing span 100 cm, vertical stabilizer span 40 cm
Weight	52 kg (dry), payload 4 kg
Batteries	Lithium sulfuryl chloride primary batteries, 24V and 10V packs, 17 MJ. Endurance up to 10 months (mission dependent)
RF data telemetry	Iridium satelite data telemetry
Operating depth range	20 to 1000m (configuration dependent)
Range	4600 km (equal to 650 dives to 1000 m depth)
Typical speed	25 cm/s
Glide angle	16° to 45°

Table 3.1: Seaglider specifications (iRobot corporation, 2012).

from the previous dive, and receives a command file with commands for the next dive (if there are no new commands from the pilot, the glider continues with previously stored commands). Then the GPS obtains a second fix and updates the estimated position. Pitch and desired buoyancy needed to reach the target depth are set at the beginning of the dive to achieve the wanted glide angle and descent rate. Then the descent starts as the external bladder of the VBD starts deflating (for a 1000 m deep dive the bladder bleeds approximately 150 cc oil back into the reservoir) and hence reducing the buoyancy of the Seaglider. At this point the data collection begins.

When the glider senses a depth greater than the target depth, the VBD inflates the bladder in order to equal the surface buoyancy from before the start of the dive, the glider pitches up and starts ascending toward the surface. As it approaches the sea surface again, the glider finishes the dive cycle by pitching down and pumping to lift the tail mast and antenna above the water.

3.1.3 Sensors

The sensors used for CTD-measurements are listed in table 3.2. Conductivity and temperature are measured by a Sea-Bird Electronics(SBE) CT Sail, an unpumped and non-ducted set of sensors designed for use on Seagliders, mounted on a small fin that penetrates the top of the fairing between the wings. An unpumped sensor consumes less power which is important when the glider is deployed for long periods of time. The relatively slow speeds and acceleartions of the Seaglider should provide a steady flow to the sensors. However, Janzen and Creed (2011) examine the CT Sail in comparison with the newer pumped SBE GPCTD (Glider Payload CTD), and CT Sail is shown to have problems with salinity spikes, especially in areas with rapid temperature change.

15

The pressure sensor (Paine® strain gauge sensor), is located inside the fairing at the front of the pressure hull. The pressure sensor output, in addition to identify the depth at which the temperature and salinity measurements belong, is used for vehicle control as well.

A depth-averaged current is estimated for each dive, though there are no sensors measuring current. Instead, the Seaglider uses the difference between a dead-reckon displacement of the dive and the actual displacement to calculate the current needed to carry the glider to the resurface location. A hydrodynamic model is used to determine the dead-reckon displacement of dives, as it estimates the Seaglider's velocity as a function of buoyancy, pitch, and water density (iRobot corporation, 2012). This method does not allow for direct current measurement at any given depth of the dive, but combined with the hydrographic data, the depth-averaged current estimate can be used to calculate an estimate of the absolute geostrophic velocity at any given depth within the depth range of the dive.

Sensor	Measurement range	Initial accuracy	Typical stability
Paine® strain gauge pressure sensor	0 - 1500 psia	±0.25% of full scale	-
SBE CT Sail temperature	-2°C to +35° C	±0.002°C	0.0002°C/year
SBE CT Sail conductivity	-	±0.002 (equivalent salinity)	0.0001/year (equivalent salinity)

Table 3.2: Sensor specifications

3.2 Data processing

3.2.1 Glider data

For each dive the glider sends .dat- and .log files back to the basestation, which consist of scientific data and a record of what happened during the dive, respectively. The basestation generates several different file formats by the data from the glider, one of which is netCDF (.nc) which captures all processed data from each dive. The netCDF files from each dive have been opened in Matlab with routines from a toolbox called nctoolbox, which allows for read-only access to netCDF files. The netCDF files were then converted to individual .mat files (which can be manipulated in Matlab) for each dive and property, e.g. temperature560001, salinity560001 (temperature, and salinity from the first dive by Seaglider560). The data extracted from the nc.-files for this study are temperature, salinity, density, depth-averaged current, time, and GPS coordinates.

16

Next the data were grouped into stations by averaging the ascending profile of one dive and the descending profile of the next. The location of the station is set at the start-coordinates of the second dive. Arranging the profiles like this allows for us to calculate geostrophic velocity at locations near the middle of each dive, the positions the depth-averaged current measurements are assigned to. The data were also sorted in 1m vertical bins where bins with multiple datapoints were averaged, and bins with missing datapoints were linearly interpolated from adjacent bins. The arranging of the data into bins is a necessary step to take before starting calculations. The stations are then sorted into transects for each journey along the target track heading north-west, and each journey south-east. In an effort to reduce noise from ageostrophic effects, all hydrographic data and depth-averaged currents have been smoothed horizontally by a three dive moving average filter.

Transect	Period	Dives (omitted dives)
1	23.05.12-08.06.12	10-80 (52-55)
2	10.06.12-03.07.12	90-162 (119-123,146)
3	04.07.12-08.08.12	168-262 (194-197,199-201,203-205,208-219,221)
4	09.08.12-30.08.12	272-328 (279,320-322)
5	01.09.12-29.09.12	376-441 (397-399)
6	30.09.12-23.10.12	443-507
7	23.10.12-18.11.12	511-576 (517,558-560,563-565,570)
8	19.11.12-15.12.12	580-642 (629-632)

Table 3.3: Details of each Svinøy section transect: Time period, dive numbers. Transects of odd numbers are heading seaward, while transects with even numbers are heading shoreward.

All stations from each indivudual transect are projected onto the same straight line between the outermost (furthest seaward) and innermost Seaglider target checkpoints of the Svinøy section. The section, or the Seaglider target-track, runs southeastward (directed toward to 137°, in compass coordinates) from its offshore limit at 65.50°N, 2.00°W. In this study when we refer to cross-track and along track directions, it is in relation to the target-track. Distance along the section (e.g. the x-axis in figure 4.2) is measured from the offshore checkpoint, increasing southeastward along the section.

Data from stations located far off- and/or stations located at large angles off the glider's target-track, as well as data from stations located near one another, have been excluded from the transects. Stations located too close to each other can lead to overestimates of velocity, while projecting stations on to the transect line which in reality deflect off the transect line by a large angle would lead to overestimates or underestimates of velocity depending on the direction of the deflection. Removing stations leaves

gaps in the depth-averaged velocity data. In most cases this has been solved by interpolating between the datapoints from before and after the excluded station(s). However, depth-averaged current from some of these omitted stations has been included where the interpolation method is thought to give unrealistic values (e.g. in areas where several subsequent stations have been removed).

After the stations are projected on to the target track, the data are linearly interpolated to 1000m horizontal intervals. In certain cases, data has been downsampled before being presented visually. All figures showing arrow plots of the current data over bathymetry maps show only every fourth datapoint along the section. Or one arrow every 4 km.

When converting to and working with the data in stream-coordinates, the actual geographic coordinates of the data are not retained (see section 2.4 for details). However, the data are inserted into the same transect and adjusted to align the core of the current with the area it is most frequently located.

3.2.2   RCM data

A data-set from an RCM-7 current meter from Aanderaa Data Instruments have been provided to be used to compare with, and verify the validity of the estimated current at 1000 m depth calculated from the Seaglider data. The RCM is positioned at 63.96°N and 1.65°E, approximately 6 km southwest of the location where the section crosses the 2000 m isobath.

The current-estimate at 1000 m depth for each of the Seagliders crossings of the 2000 m isobath has been compared to the component of the RCM-measured current at 1500 m depth that corresponds to the cross-track direction of the section (See figure 3.2). We assume the baroclinic contribution to the current to be negligible at 1000 m depth and deeper, thus the current at 1000 and 1500 m depth should be equal. The RCM-data is a true time series in one location, while the velocity at 1000 m is not from one position alone, rather the velocity from 10 km surrounding the 2000 m isobath in both directions along the transect. The red line in each of the plots represents the point in time the glider crosses the 2000m isobath. The nature of the saw-blade trajectory of the glider makes it so that we can not pinpoint the time exactly, as the Seaglider records time data only before and after dives. Therefore the inclusion of velocity data within the 10 km of the transect before and after the crossing of the 2000 m isobath (equal to the length of 4-5 typical dives) have been utilized in these comparisons to at least identify the velocity at 1000 m within a relevant time frame and vicinity close to the RCM-measurements. The time period of the plots is the period taken for the glider to travel the 20 km. A 13 hour moving average filter was applied to the RCM-data to remove the tidal influence on the current.

The comparison reveals an agreement between the direction of the current at the two depths. The magnitude of the current does not always compare entirely. Transect 2,

18

transect 3 and transect 4 (Figure 3.2b, 3.2c, and 3.2d) all show lower velocities at 1000 m, while transect 1 and transect 6 (Figure 3.2a, and figure 3.2f) show higher velocities at 1000 m.

(a) Transect 1

(b) Transect 2

(c) Transect 3

(d) Transect 4

(e) Transect 5

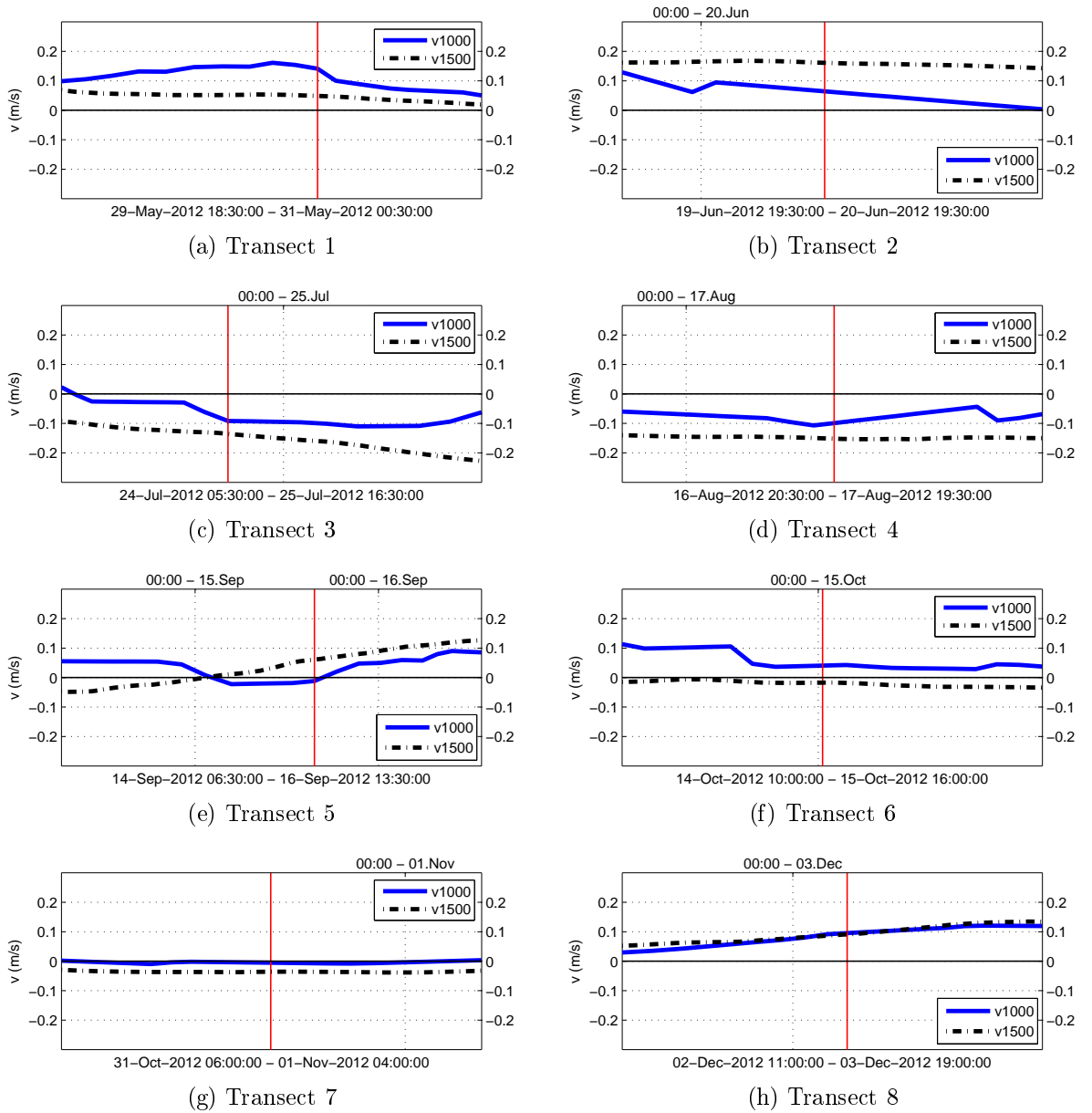(f) Transect 6

(g) Transect 7

(h) Transect 8

Figure 3.2: Comparison between cross track velocity estimates at 1000m depth from Seaglider-data, and measured RCM velocity in the corresponding direction at 1500 m depth. The red line represents the time when the Seaglider crosses the 2000 m isobath.

20

Chapter 4

Results

4.1 Hydrography

The hydrography of the section is dominated by warm saline AW overlying colder and less saline NSDW. As can be seen from the TS diagram in figure 4.1, there is also a contribution from relatively warm masses with salinities lower than the AW, and temperatures between $5°C$ and $13.5°C$. These properties are mostly connected to relatively shallow patches of NCW, but surface water near the offshore end of the section also exhibit similar properties (e.g. figure 4.2e and 4.2f). The AW mostly has temperatures between $4°C$ and $12°C$ and salinities between 35 and 35.4. The NSDW has temperatures between -1$°C$ and $4°C$ and salinities mostly between 34.9 and 35.
The sub surface Polar Front can be identified in most transects, with the exception of transect 5 and 8, by a rather distinct steepening of the isothermal, isohaline and isopycnal surfaces and an accompanying strong current located in an area of transition between the warm, saline AW and the cold and comparatively fresh NSDW. To illustrate, transect 2 and 6 (figure 4.2b and 4.2f) show examples of rather distinct fronts.

The spatial distribution of the different water masses in the section varies, but typically the AW occupies most of the the upper 400 - 500 m of the water column shoreward of the front, while the rest of the water column is occopied by NSDW. AW is also found seaward of the frontal region. However,it is found in a thinner layer near the surface, usually extending down to between 100 m and 150 m depth. The extent and amount of AW, as well as the hydrographic structure seaward of the front, varies. In transect 1, 2 and 4 (See figure 4.2a,4.2b and 4.2d) we observe a continuous slab of AW covering the extent of the transect seaward of the front, while in transect 5, 6, and 7 (See figure 4.2e, 4.2f, and 4.2g) the AW found seaward of the front is located in eddy-like features.
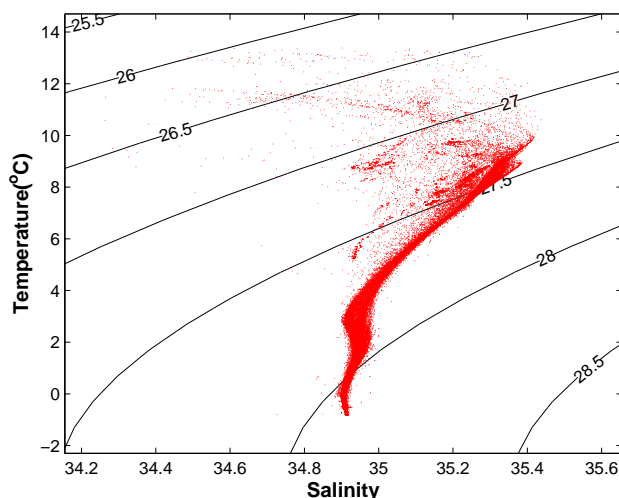
Figure 4.1: Temperature-salinity diagram of all transect data. Contours are lines of constant density, $\sigma_t = \rho - 1000$ (kg/m^3).

The freshest near-surface water masses are found most abundantly in transects 5-8 which extend further into the NS than transects 1-4. Typically in the upper 50-100 m of the water column, either in the mixed layer, e.g. seaward of the front in transect 5 and 6 (See figure 4.2e and 4.2f), and the 30 first km along transect 7 and 8 (See left of 50 km in figure 4.2g and 4.2h). In transects 1-4 the freshest near-surface water masses are found in thinner layers overlying the AW.

The structure and position of the front also varies substantially (The variation in the position of the front is presented in figure 4.6 in section 4.4). As mentioned in section 2.4, the point where the 1027.6 kg/m^3 isopycnal surface crosses 200m depth has been chosen as the identifying factor for the location of the Polar Front. This reference point for the front is necessary when converting into stream-coordinates. The temperature at this point varies between transects by a few tenths of a degree around an average of $6.5°C$ while the salinity values range from 35.13 to 35.17. The furthest seaward the front (according to our definition) is observed is in transect 8 in November/December when it is located above the 2600 m isobath (See the black circle in figure 4.3h). The innermost it has been located is in transect 1 in May/June at when it is located above the 1800 m isobath, 90 km further shoreward (See black circle in figure 4.3a). On average, when considering its location along the section, the Polar Front is located roughly 15 km seaward of the 2000 m isobath.
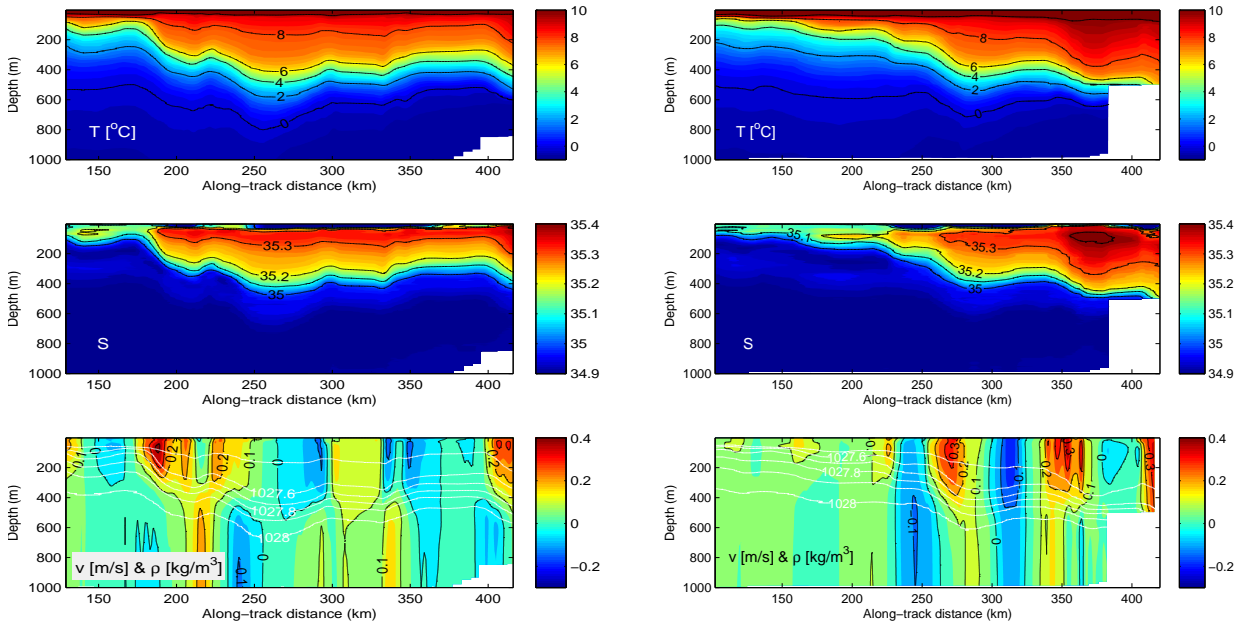
The structure of the front manifests itself predominantly in one of two ways: with a sharp horizontal density gradient, or as a wedge structure with linearly rising isopycnal surfaces seaward and an indistinguishable front, e.g. transect 6, and transect 8, respectively (See density contours in figure 4.2f and 4.2h).
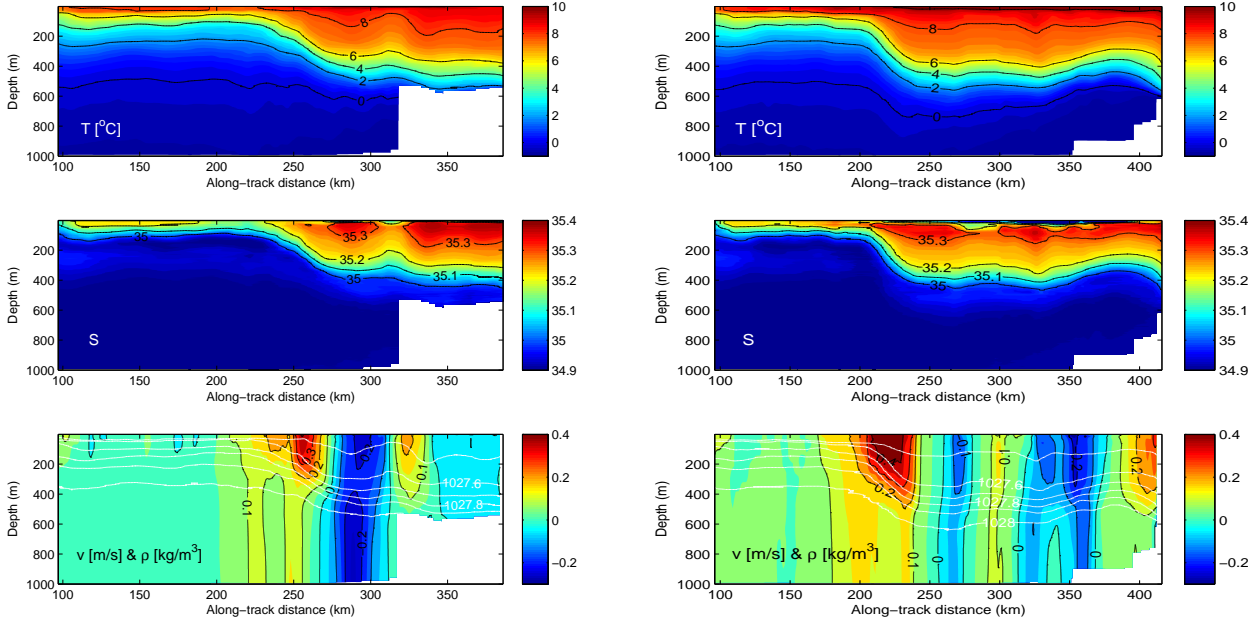
(a) Transect 1 (May - June)

(b) Transect 2 (June - July)

(c) Transect 3 (July - August)

(d) Transect 4 (August)

Figure 4.2: Hydrographic- and velocity-profiles of transect 1 - 4 (a - d). Temperature ($°C$) profiles are displayed in the upper panels, salinity profiles in the middle panels, and white density (kg/m^3) contours over total geostrophic velocity (m/s) profiles in the bottom panels. The profiles run from northwest to southeast (left to right).
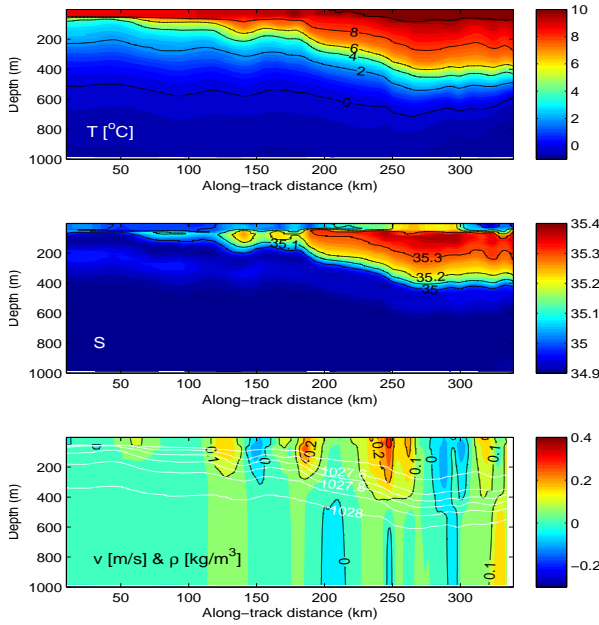
(e) Transect 5 (September)
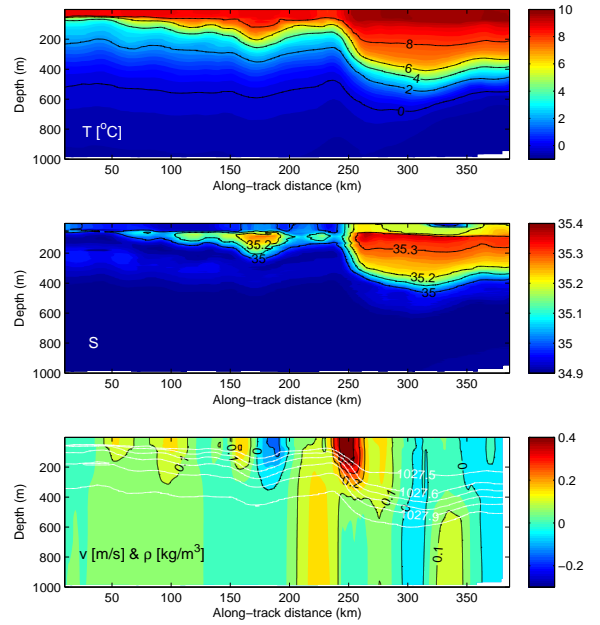
(f) Transect 6 (September - October)
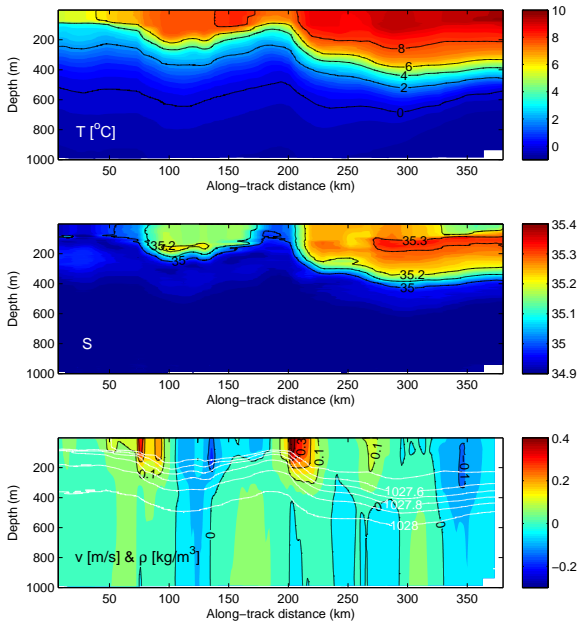
(g) Transect 7 (October - November)

(h) Transect 8 (November - December)

Figure 4.2: (cont.): Hydrographic- and velocity-profiles of transect 5 - 8 (e - h)

4.2 Current

Figure 4.3 shows the depth-averaged current as projected onto the Seaglider target-track (See section 3.2.1 for target-track description).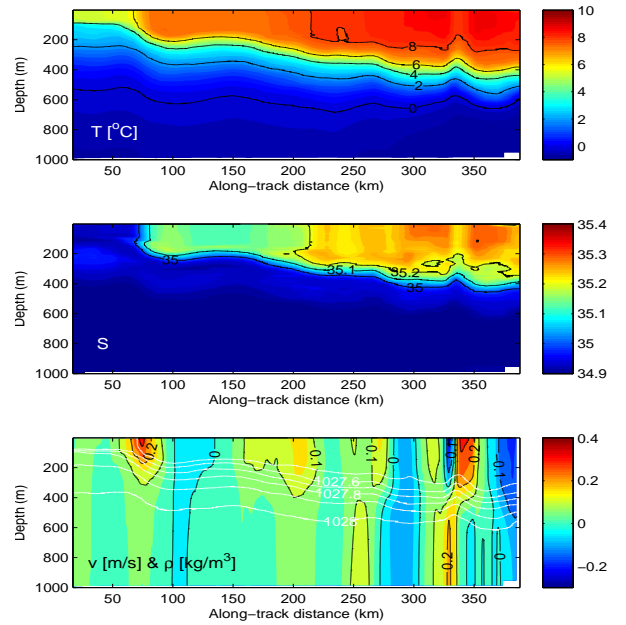 For each transect we can see spatial variations as well as temporal variations between them. In some portions of the transects there are strong currents limited to relatively narrow bands, and other places almost laterally uniform current over a large area, e.g. transect 1, shoreward and seaward of the 2000 m isobath, respectively (See figure 4.3a). Between the 500 m and 1000 m isobaths in all the transects that cover this area, we see a strong current (See figure 4.3b,4.3c, and 4.3d). This area is considered part of the eastern branch of the NwAC (this will be commented on further in section 4.3). In the vicinity 1000m isobath there is typically very low cross-track velocities, except for a negative values in transect 8 (Figure 4.3h). Between the 1000 m and 2000 m isobaths, the current displays less consistency. The location of the Polar Front, and thus the NwAFC, is variable and is usually found between the 2000 and 2500 m isobaths (The location of the Polar Front is marked by a black circle on each individual transect in figure 4.3). The depth-averaged current is typically strong in the vicinity of the NwAFC. Seaward of the front, the depth-averaged current is typically less variable, except for the areas where we observe eddy-like features in the hydrographic- and geostrophic current data. An example of this can be seen in the upper 200 m of the water column, seaward of the front in transect 7, where a mass of AW enclosed by less saline water rotates in an anti-cyclonic eddy (Figure 4.2g). Individual transects, e.g. transect 1, 2, and 3 (See figure 4.3a, 4.3b, and 4.3d), have areas of substantial negative cross-track depth-averaged currents. However, looking at figure 4.4a we see that the prevailing current direction of the depth-average current for all the transects is northeastward, which corresponds to a positive cross-track velocity relative to the section. The depth-averaged current most frequently has a magnitude between 5 and 15 cm/s. Measurements with nearly along-track (northwest and southeast) or negative cross-track (southeast) velocities are comparatively sparse.

The highest calculated geostrophic velocity is found in the core of the NwAFC in transect 6 (Figure 4.2f) where the velocity near the surface reaches 54 cm/s. Typically the velocity in the core of the NwAFC exceeds 40 cm/s with the exceptions being in transect 5 and 8 (Figure 4.2e and 4.2h). Transect 2, 3, and 4, which extend the furthest shoreward, capture the edge of the NwASC where the currents are fairly strong as well (See figure 4.2b,4.2c, and 4.2d). Below 400 m depth, the calculated geostrophic velocities rarely exceed ±0.2 m/s. However, the calculated total geostrophic velocity at 1000 m is not insignificant, at times exceeding 10 cm/s. The highest geostrophic velocity calculated at maximum dive depth is in transect 1 where the the negative cross-track velocity reaches 26 cm/s approximately 40 km shoreward of the front (See figure 4.2a).

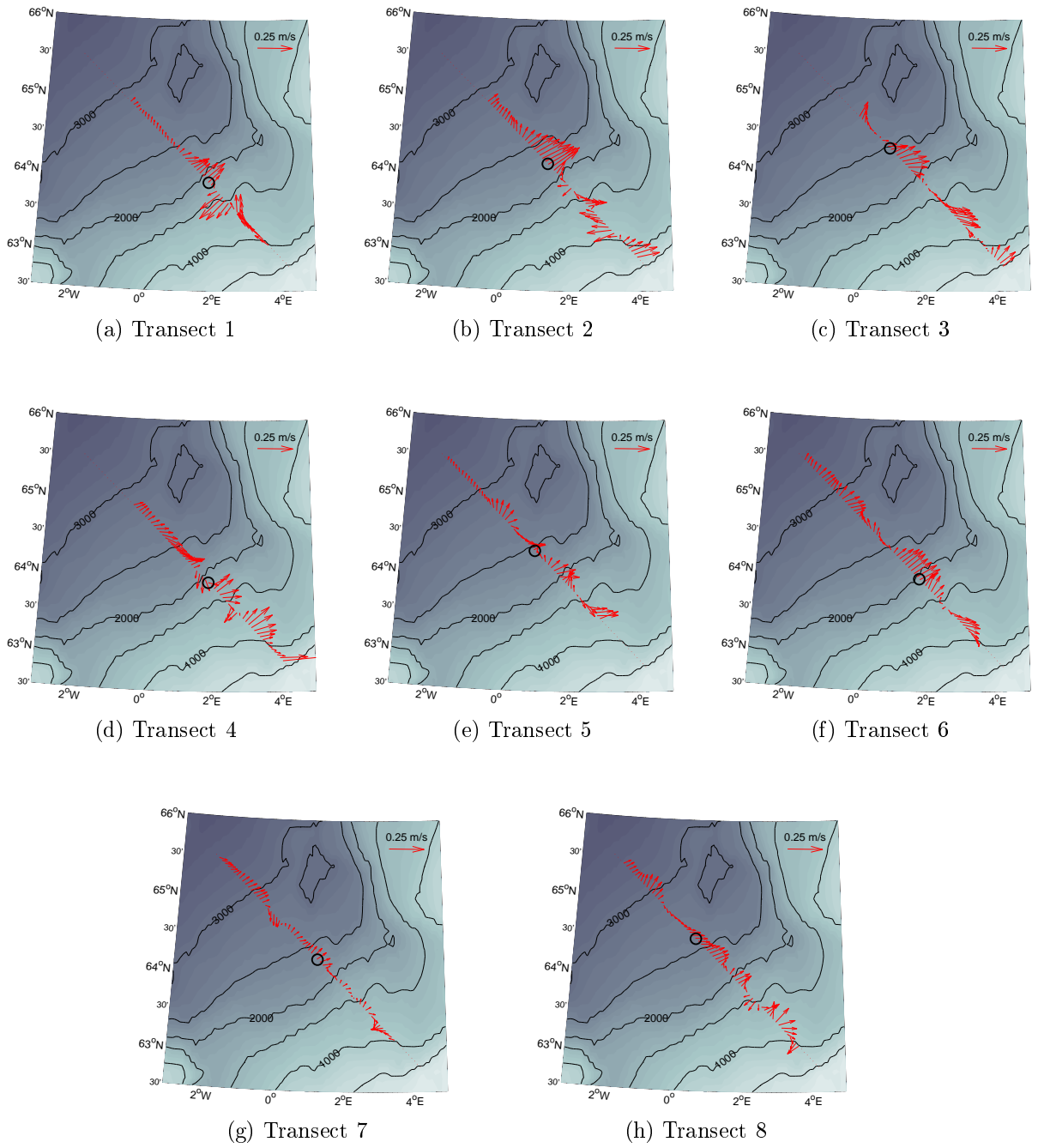(a) Transect 1   (b) Transect 2   (c) Transect 3

(d) Transect 4   (e) Transect 5   (f) Transect 6

(g) Transect 7   (h) Transect 8

Figure 4.3: Arrow plots (over a bathymetry map) of the depth-averaged current for transect 1-8 (a-h).

Figure 4.4b shows the distribution of the direction and magnitude of the flow measured by RCM (See section 3.2.2 for details on RCM-data) at 1500 m depth during the time period of the glider mission. The flow at this level is most frequently directed northeast and southwest, along the slope of the topography. The maximum measured speed at 1500 m depth is 28 cm/s, while the mean speed is 10.8 cm/s. Estimated current speed at 1000 m depth in the vicinity of the RCM is not as high, with a maximum speed of 16.1 cm/s and a mean speed of 6.4 cm/s.
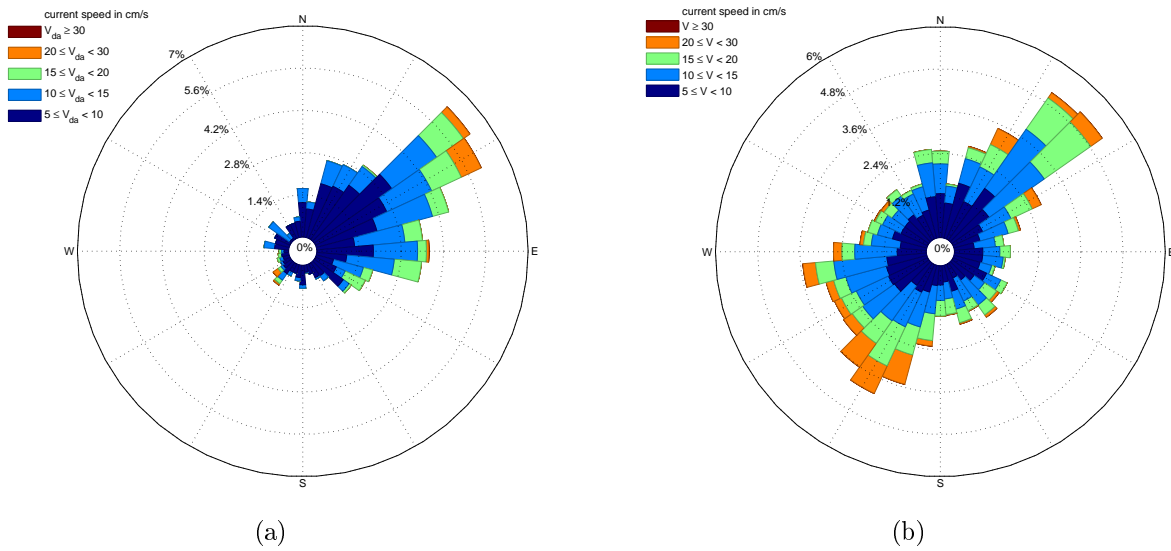

Figure 4.4: Frequency distribution of direction and magnitude from the Seaglider depth-averaged current estimates (a), and the current at $1500m$ depth from RCM-mooring located above the $2000m$ isobath (b).

4.3 Transport

Transport estimates for the western branch of the NwAC are displayed in figure 4.5 and table 4.1. Orvik et al. (2001) found the offshore limit of the eastern branch of the NwAC to be near the 1000m isobath where they found the vertically integrated transport to be very small. For the sake of comparison with the estimates from Høydalsvik et al. (2013), who calculated transport seaward of the 1100 m isobath, we have limited our estimates to cover the same portion of the section. The average total transport of AW is 4.7 Sv, while the minimum and maximum transports are 2.1 Sv and 6.5 Sv, respectively. On average the contribution from the baroclinic and barotropic components of the transport are nearly even, with the average barotropic transport of 2.6 Sv contributing roughly 55 % of the total transport, and the average baroclinic transport of 2.1 Sv contributing

the remaining 45 %. The barotropic transport varies from a minimum of -0.5 Sv to a maximum value of 4.1 Sv. The baroclinic component of the transport varies between a minimum value of 1.1 Sv and a maximum of 3 Sv.

Transect Number	1	2	3	4	5	6	7	8	Average
Transect length	258	259	226	253	312	345	348	338	292.4±48.7
Area of AW	56.9	71.8	70.6	61.2	75	66.6	81.3	88.8	71.5±10.4
AW transport	2.1	4.8	5.1	5.1	5.9	5.4	2.4	6.5	4.7±1.6
AW barotropic transport	-0.5	3.2	4.1	2.5	3.6	3.7	0.6	3.5	2.6±1.7
AW baroclinic transport	2.6	1.6	1.1	2.7	2.4	1.7	1.9	3	2.1±0.7

Table 4.1: Volume transport details for the western branch of the Norwegian Atlantic Current (seaward of the 1000 m isobath). Transect length [km] , Area of AW [km^2],and transport [Sv]. The presented error of the average transport is the standard deviation.
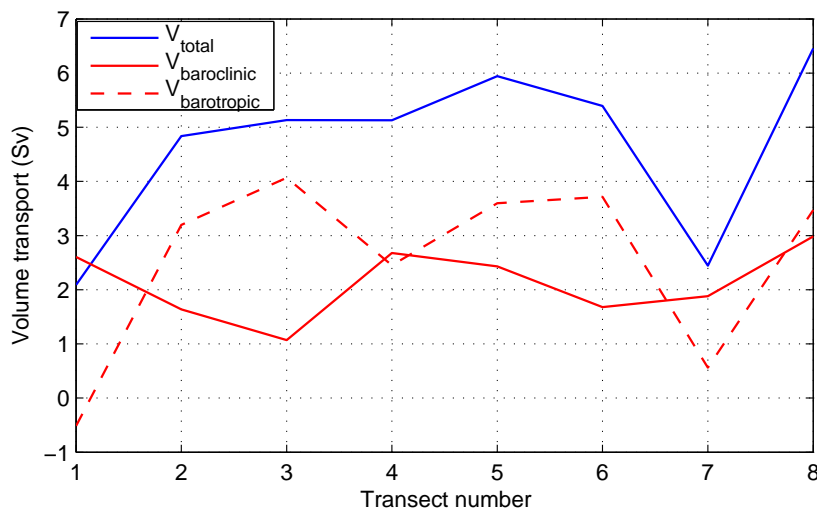
Figure 4.5: Cross-track volume transport of AW for each individual transect. V_{total} (Sv), $V_{barotropic}$ (Sv), and $V_{baroclinic}$ (Sv) are the total transport, and the barotropic- and baroclinic component of the transport, respectively.

4.4   Eularian- and stream-coordinate averaging

Figure 4.7 shows the results of Eularian- and stream-coordinate averaging of hydography and depth-averaged current and the geostrophic velocity resulting from the average density fields. The stream-coordinate average fields are, technically, not representable

Figure 4.6: Location of the chosen stream-coordinate origin (arrows) for each transect in relation to the average location of the Polar Front (dashed line).

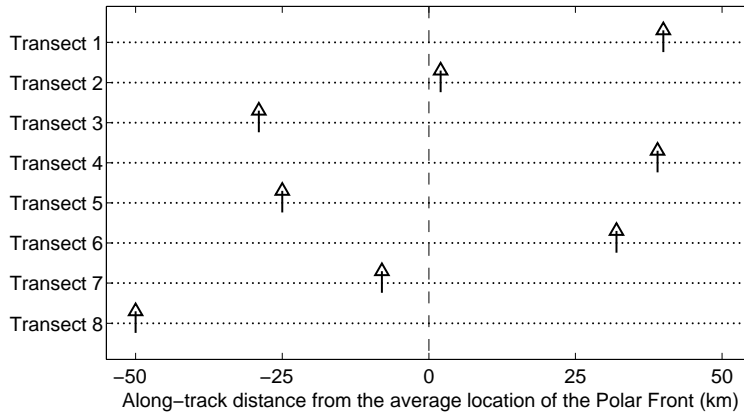in geographic space like the Eularian averages, but have been plottet along the same portion of the section for the sake of comparison. The Eularian average fields are limited to a 250 km long portion of the section (from 100 km to 350 km along the section measured from the northwest), because this area was covered nearly completely by all transects. Additionally, the western branch of the NwAC, in accordance to the inner limit at the 1100 m isobath used in section 4.3, does only stretch a few more km shoreward. As described in section 2.4, the transects are shifted so that the origin for each transect aligns with the rest before the temporal averaging is applied. So, while the stream-coordinate average field is also limited to a width of 250 km, it actually includes data from a 340 km wide area along the section. The location of the Polar Front, i.e. the stream-coordinate origin as identified by the 1027.6 kg/m^3 isopycnal surface crossing at 200 m depth, for each transect in relation to the average position of the front (220 km along the section) is presented in figure 4.6. The position of the front changes substantially between transects, usually by several tenths of kilometers.

Overall, the temperature, salinity and density values are very similar. However, the resulting hydrographic structure in the frontal region varies quite significantly between methods. We can see a more pronounced tilt of the isothermal, isohaline, and isopycnal surfaces in the stream-coordinate average fields, resembling the individual transect profiles with more distinct fronts like transect 2 and 6 (Figure 4.2b and 4.2f). The 1027.6 kg/m^3 isopycnal surface drops 150 m in 40 km in the stream-coordinate average field. An equal drop of the same surface in the Eularian average field spans a horizontal area of 80 km. The resulting geostrophic current estimates, in stream-coordinates, reveals a stronger and more concentrated current core (we define the core as the part of the transect with velocities exceeding 10 cm/s), an approximately 40 km wide baroclinic jet with a maximum velocity of 31.5 cm/s (figure 4.7d). The Eularian averaging results

29

show a weaker current core, smudged out over an area nearly double the width of that observed in the stream-coordinate average field. The maximum velocity of 18.3 cm/s, is equal to the average velocity in the stream-coordinate current core, while the average velocity in the Eularian current core is 13.4 cm/s.

The area of the stream-coordinate current core is 12,51 km^2, out of which 10.49 km^2 is occuipied by AW. The Eularian current core area is, in accordance with the width, approximately double that of the stream-coordinate core at 24.2 km^2, out of which 21.56 km^2 is occupied by AW. If we consider only the part of the current core occupied by AW, the average temperature in the stream-coordinate and Eularian average field is 7.4°C and 7.2°C, respectively, while the average salinity is 35.16 in both cases.

Total AW transport in the entire average-field is 4.8 Sv and 4.9 Sv for the stream-coordinate- and Eularian fields, respectively. If we consider only the current cores, the numbers are 2.1 Sv and 3 Sv. The baroclinic component of the transport, in the stream-coordinate current core, is 1.6 Sv and accounts for approximately 80% of the total transport. The remaining 20 % from the barotropic component is to 0.4 Sv. The larger Eularian current core has a baroclinic contribution to the transport of 1.8 Sv, which is equal to approximately 60 % of the total transport, and a barotropic contribution of 1.2 Sv contributing the remaining 40 %.
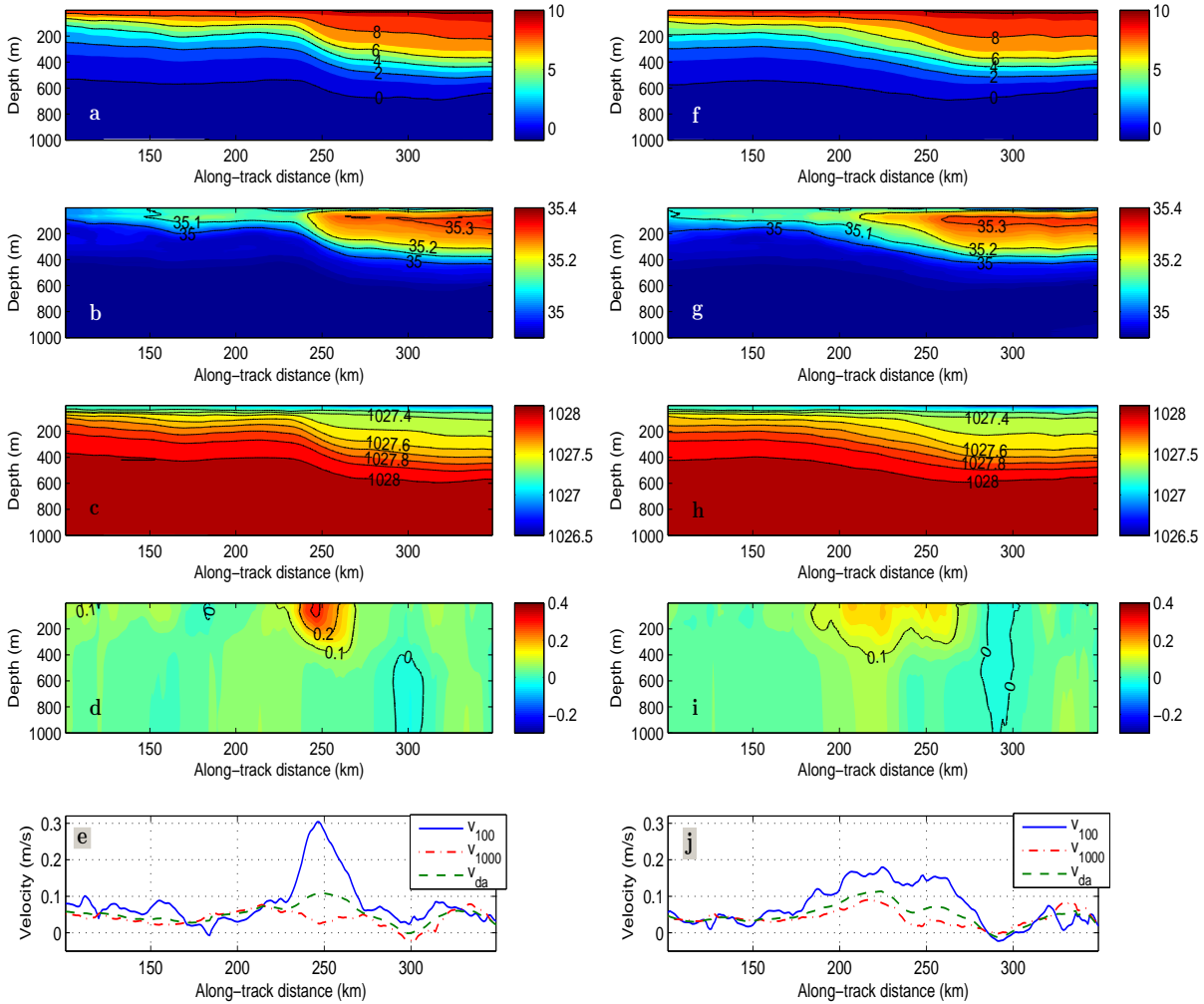
Figure 4.7: Stream-coordinate average fields (a-e), and Eularian average fields (f-j). (a) and (f): Temperature (°C); (b) and (g): Salinity; (c) and (h): Density (kg/m³);(d) and (i): Absolutel geostrophic velocity (m/s); (e) and (j): Depth-averaged velocity and absolute geostrophic velocity at 100 and 1000 m.

Chapter 5

Discussion

5.1 Stream-coordinate average

The stream-coordinate averaging has proved successful in removing the effects of the meandering of the NwAFC, leaving mostly variations in the actual structure of the Polar Front to affect the averaging, and subsequently a more focused and accurate rendition of the average state of both the front and the accompanying current than that resulting from Eularian averaging. Our stream-coordinate average yields a baroclinic frontal jet approximately 40 km wide and approximately 400 m deep when we define the current as the area with velocitiy exceeding 10 cm/s. Comparatively, our Eularian averaging yielded a current more than twice the width, using the same definition of the current core. However, looking at figure 4.7i and the geostrophic velocity at 100m in figure 4.7j, we can see that the Eularian averaging has in fact resulted in a collection of multiple velocity maxima within this 80 km wide area. Høydalsvik et al. (2013) describe a well defined single current core 50 km wide, and 400 m deep resulting from Eularian averaging of 9 transects along the Svinøy section. If we apply the same definition of the core as for our estimates, however, the core presented is in fact roughly 80 km wide like our Eularian average. The data presented in Høydalsvik et al. (2013) have a lower resolution than our data, as they applied a 10-dive moving average filter, which yielded a horizontal resolution of between 30 and 70 km (depending on the horizontal displacement of the dives). The data in this study was applied a 3-dive moving average filter, which results in a resolution of 9 to 21 km in order to avoid excessive smoothing before applying the different averaging methods. This has left our Eularian average field looking less smooth than that of Høydalsvik et al. (2013).
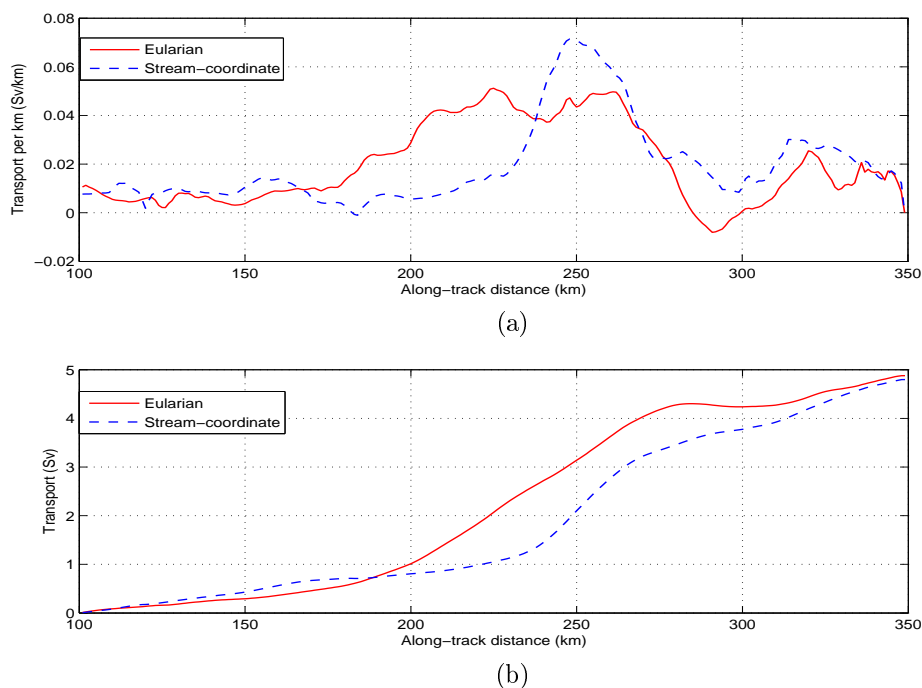
Figure 5.1: Vertical integrated transport per kilometer (Sv/km) (a) and Total cumulative transport of AW (Sv) along the section (b)

The vertically integrated transport per kilometer and the cumulative transport along the section are presented in figure 5.1. The vertically integrated transport along the section (figure 5.1a) reflects the calculated geostrophic velocity at 100 m to a great extent(See figure 4.7e and 4.7j). The largest AW transport per km is concentrated in the frontal region both in the case of the Eularian and stream-coordinate average. Looking at figure 5.1b we can see that the vast majority of the AW transport in the western branch of the NwAC is focused within the vicinity of the core of the NwAFC as there is a rather rapid increase in the transport in this area. Transport seaward of the frontal region is approximately 0.7, and 1.1 Sv in the case of the Eularian and stream-coordinate field, respectively. This is simply due to the fact that the area considered as seaward of the front is larger area in the stream-coordinate average field, and since the depth-averaged current in this area is relatively similar in the case of both Eularian- and stream-coordinates, the transport contribution in this area is larger. Although current speed seaward of the front is not necessarily lower than that found shoreward of the current core, transport per km in this area is relatively low due to the AW not extending as deep into the water column as it does shoreward of the current core. The transport shoreward of the current core in the stream-coordinate average field is approximately 1.4 Sv, while the Eularian equivalent is approximately 1 Sv.

A rough calculation of the size of the current core of the NwAFC in each individual

transect using the same definition as before (Includes all AW with positive cross-track current velocity larger than 10 cm/s within a 80 km range centered in the stream-coordinate origin for the transect) yields an average core area of 12.28 km^2. This number is close to the size of the stream-coordinate current core of AW which has an area of 10.49 km^2. The area of the Eularian current core is substantially larger at 21.56km^2. The AW transport in the core of the NwAFC from individual transects varies from 1.2 Sv in transect 5, to 4.6 Sv in transect 2, and has a mean value of 2.6 Sv (See transport details in table 5.1). The average total transport is slightly closer to the Eularian average transport of 3 Sv, than the stream-coordinate transport of 2.1 Sv. However, the average transport per square kilometer is 0.20 Sv/km^2 which is nearly very close to the stream-coordinate value of 0.19 Sv/km^2 compared to the Eularian average of 0.14 Sv/km^2. The average temperature and salinity calculated from individual transects, is 7.45°C and 35.18, respectively. Average temperature and salinity of the core in stream-coordinates is 7.36°C and 35.16, while the Eularian averages are 7.20°C and 35.16. This result demonstrates the advantage of the stream-coordinate averaging well, as it reflects the state of the current core very accurately in comparison to the Eularian average.

Transect Number	1	2	3	4	5	6	7	8	Average
Area of AW	10.4	15.1	13.2	14.9	7.8	17.9	7	12	12.3±3.8
AW transport	2.3	4.6	2.8	2.8	1.2	3.8	1.5	1.5	2.6±1.2
Transport per km^2	0.22	0.3	0.21	0.19	0.15	0.21	0.22	0.13	0.2±0.05

Table 5.1a: Transport details in the core of the NwAFC from individual transects. Area of AW (km^2), transport (Sv), and transport per km^2 (Sv/km^2)

Averaging method	Eularian	Stream-coordinate
Area of AW	21.6	10.5
AW transport	3	2.1
Transport per km^2	0.14	0.19

Table 5.1b: Same as table 5.1a, only details for the current core of the Eularian, and stream-coordinate average fields.

5.2 Sources of error

5.2.1 Error sources related to the Seaglider

As previously mentioned in section 3.1.3, the conductivity and temperature data from Seagliders using the CT Sail, have been shown to produce salinity spiking, especially

in regions of rapid temperature change. This is a result of the conductivity sensor and thermistor not being connected (ducted), therefore the water sample measured by the one sensor may not be identical to the sample measured by the other. The conductivity sensor also has a protecive metal guard, which may reduce flushing and further enhance the errors (Janzen and Creed, 2011). In mapping larger-scale hydrographic features of the water column, however, Janzen and Creed (2011) found the CT Sail to produce results in qualitative agreement with the pumped and ducted SBE GPCTD. Uncertainties regarding the transport estimates stem mostly from errors in the depth-averaged velocity.

The depth-averaged current has an uncertainty of approximately 1 - 1.5 cm/s (Eriksen et al., 2001). As mentioned in section 3.1.3 the depth-averaged current estimates rely on a dead-reckon displacement determined after each dive. This displacement is based on a hydrodynamic model, the accuracy of which is the source of the error in the current estimates. A consistent and one-directional error directed exactly across the section, of 1.5 cm/s across the entirety of our average AW domain of approximately 79 km^2, would result in a transport error of nearly 1.2 Sv, which is substantial.

5.2.2   Errors related to stream-coordinate averaging

The quality of the results of the stream-coordinate averageing is reliant on the accuracy of the chosen identifying factor of the feature one wishes to study. In the case of this study the location where the 1027.6 kg/m^3 isopycnal crosses 200 m depth was found to be representative for the position of Polar Front and the center of the NwAFC to within a few km for most transects. In the case of transect 8, however, there is no distinct horizontal density gradient to mark the location of the front which is usually the case (See density profile in figure 4.2h). The stream-coordinate origin for transect 8 was still adjusted according to the same identifying factor as the rest, though there is no distinct frontal structure or current core in this exact location. The origin set for transect 8 is the origin positioned furthest seaward of all the transects at 50 km northwest of the average position of the front. If multiple transects would exhibit similar hydrographic structures as transect 8, where the location of the feature we wish to study is not necessarily evident, this would be a source of uncertainties in the accuracy of the final stream-coordinate average. Since transect 8 is the only case of this problem in this study, the final stream-coordinate should reflect the actual average state of the current core well.

As mentioned in section 2.4, we have applied a simplified form of stream-coordinate conversion where we do not rotate the transects according to the downstream direction because we do not have direct current measurements of the current core. Hence we can not identify the direction of the current at any specific depth, only the direction of the depth-averaged current is estimated. Figure 5.2 shows the distribution of the depth-averaged current direction and magnitude in the vicinity of the stream-coordinate origins
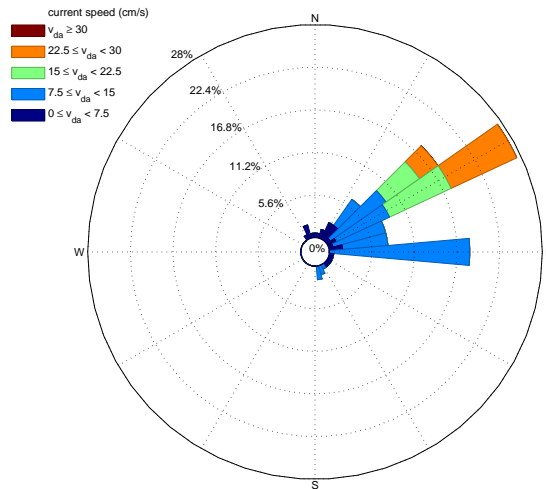
Figure 5.2: Frequency distribution of direction and magnitude of the depth-averaged current near the stream-coordinate origin (± 10 km along track from origin) for all transects.

(i.e., in the vicinity of the core of the NwAC) . The strongest currents (with magnitude greater than 15 cm/s) are directed northeast between 45° and 65°. The cross-track direction in relation to the section is approximately 47°, i.e. the strongest currents are directed between -2° and 22° in relation to a positive cross-track current. A 22° deflection off the cross-track direction would make the cross-track component 6% smaller than the actual magnitude of depth-averaged current.

If we consider the direction of the depth-averaged current as representative for the direction of flow in the core of the NwAFC, this 6% decrease in the magnitude of the flow related to our simplified stream-coordinate conversion is equal to a 0.6 cm/s decrease in magnitude of the average barotropic velocity component in the vicinity of the current core. Compensating for this results in an increase of transport of AW in the current core of nearly 6% (2.03 Sv to 2.15 Sv), as the size (area with total geostrophic velocity greater than 10 cm/s) increases along with the velocity. If we assume the core does not change in size, the increase in transport becomes approximately 3% from the increased velocity alone. These errors related to not rotating the transects before averaging are relatively small, but they are not insignificant. A complete stream-coordinate conversion would therefore be slightly more accurate in resolving the average velocity field.

5.3   Current and transport

Our transport estimates of AW (See table 4.1 and figure 4.5 in section 4.3) , with a mean value of 4.7 Sv and a standard deviation of 1.6 Sv show a lower and more variable

transport than the results from Høydalsvik et al. (2013) of 6.8 Sv with a standard deviation of 1.1 Sv. The barotropic component of the transport, on average, accounts for 55 % of the total transport, the results from Høydalsvik et al. (2013) show a 53 % barotropic contribution. Looking at figure 4.5 we can see that the changes in the total transport from one transect to the next are greatly affected by the changes in the barotropic component of the flow, more so than the less variable baroclinic component. This result suggests that previous transport estimates of the NwAFC in the Svinøy section reliant on a level of no motion (Orvik et al., 2001; Mork and Blindheim, 2000), are indeed quite substantial underestimates of the total transport.

Our calculated cross track current at 1000 m show an average velocity of 3.8 cm/s in the positive cross-track direction (5.4 cm/s if we consider only the average current speed, independent of direction), and maximum velocity exceeding 20 cm/s in both directions. This result is verified by the RCM data from 1500 m (see figure 4.4b) which is located in an area where the average measured current velocity is 10.8 cm/s. Furthermore, our comparison between the estimated geostrophic velocity at 1000 m depth and RCM-measured current at 1500 m depth (See figure 3.2) shows an overall agreement in current direction and to a lesser extend current speed. This suggests that our velocity estimates at 1000 m depth are in fact reasonable estimates, and thereby that the estimated contributions of a barotropic component of the transport in the Svinøy section are reasonable as well.
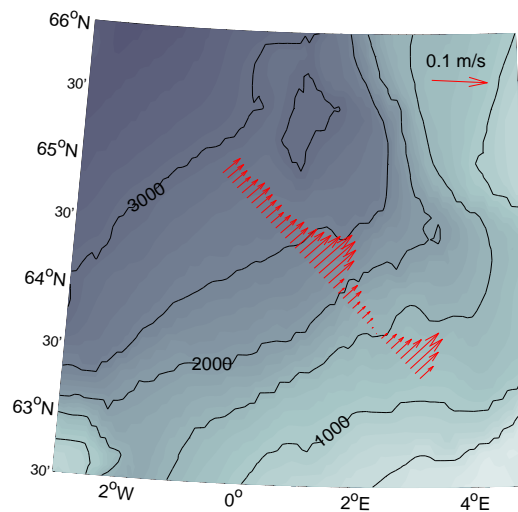

Figure 5.3: Arrow plot of time averaged cross-track velocity at maximum dive depth (1000 m)

The mean mid-depth and near-bottom circulation in the Norwegian Basin has been shown to follow a cyclonic pattern (Voet et al., 2010; Nøst and Isachsen, 2003). Using

profiling Argo floats at depths of 1000 - 1500 m in the basins of the Nordic Seas, Voet et al. (2010) found a topographically steered cyclonic circulation in the Norwegian Basin with intensified flow near the rim of the basin. The time-averaged mid-depth flow near the rim of the basin in the vicinity of the Svinøy Section moves northeast (comparable to a positive cross-track flow in our transect coordinates) at nearly 5 cm/s. Model results from Nøst and Isachsen (2003) indicate similar flow near the bottom of the Norwegian Basin. Our Eularian time average cross-track velocity at 1000 m depth is presented in figure 5.3. The average velocity is 4 cm/s, which is comparable with the results from Voet et al. (2010). There is however a distinctive increase in velocity between the 2000 - and 2500 m isobath (in the vicinity of the average position of the NwAFC), where the maximum velocity reaches 9 cm/s. A similar, though less pronounced increase in velocity at depth can be seen in the same area in Høydalsvik et al. (2013).

Mork and Blindheim (2000), calculating the volume transport of water with temperature higher than 1°C in the Svinøy section, found the average baroclinic winter-, spring- and summer transport in the western branch of the NwAC (covering an area stretching from the 1200 m isobath and 200 km seaward) to be 4.1 Sv, 2.5 Sv, and 3.7 Sv, respectively. Our average baroclinic transport of AW (water with salinity greater than 35) is 2.1 Sv, lower than all seasonal averages estimated by Mork and Blindheim (2000), however, adjusting our transport calculations to include all water with temperature higher than 1°C we obtain an average baroclinic transport of 2.7 Sv. The average baroclinic transport calculated by Høydalsvik et al. (2013) and Orvik et al. (2001) of 3.2 and 3.4 Sv, respectively, are also relatively high but comparable with the results of this study.

The temporal coverage and sample size of this study, as well as that of Høydalsvik et al. (2013) (8-9 transects covering approximately half a year), is rather limited relative to Orvik et al. (2001); Mork and Blindheim (2000) who based their calculations on data collected over several years. Therefore, it is beyond the scope of this study to make any conclusions about the seasonality of the AW transport and the quantitave results of the transport in general. Our focus is rather the applicability of the methods we utilize.

Our estimated average transport in the western branch of the NwAC of 4.7 Sv, though low in comparison to the 6.8 Sv average from Høydalsvik et al. (2013), is high in relation to the 7.6 Sv transport of AW across the Iceland-Scotland Ridge (split between the two major inflow branches) found by Østerhus et al. (2005). Orvik et al. (2001) found an average transport of 4.2 Sv in the in the eastern branch of the NwAC, which if we add to our average transport estimate becomes a total transport of the NwAC in the Svinøy section of 8.9 Sv. The definition of AW as all water masses with salinity greater than 35 may be imprecise in the southern Norwegian Ocean. As the AW enters the Norwegian Basin with salinity greater than 35.2 and on it's way toward the Svinøy section entrains and mixes with cold NSDW with salinity of 34.9. Much of the water included in our transport estimates as AW, therefore may not be actual AW at all, but rather a mix of AW and NSDW. Høydalsvik et al. (2013) found, by changing the AW definition to all water with temperature higher than 7.5°C, a transport in both

the western and eastern branch of the NwAC in the Svinøy section to be 2.8 Sv, which closely reflected the estimates of Atlantic Inflow from Mauritzen et al. (2011). If we apply the same definition we get an average transport of 2.7 Sv, and if we change the definition again to include both these identifying characteristics (salinity greater than 35 and temperature greater than 7.5°C) in order to remove warm fresh near surface water, our average transport estimate becomes 2.6 Sv.

Chapter 6

Concluding remarks

Hydrographic and current data obtained by Seaglider in the Svinøy section in the Norwegian Sea during a period from May to December of 2012 has been used to investigate the applicability of stream-coordinate averaging of the NwAFC, an unstable baroclinic boundary current located in the Polar Front. Additionally, transport estimates of AW in the western branch of the NwAC based on calculations of absolute geostrophic velocity have been addressed.

When studying hydrographic structure and hence the geostrophic velocity field of a section, the Seaglider's high horizontal resolution is a great advantage over the traditional CTD-survey from a research vessel. A high horizontal resolution is important when studying a meandering feature like the NwAFC and the Polar Front, which are relatively narrow features that can be positioned within a wide area. A CTD-survey of a long section like the Svinøy section would be comparatively costly, and even more for a high resolution horizontal grid with stations only a few km apart. The average horizontal resolution (dive distance) in our transects is 5.6 km. The horizontal dive distance can be adjusted to as low as 2 km of dead-reckoning displacement for a 1 km deep dive. However, a very high horizontal resolution like this comes at the expense of the total mission range.

The most limiting aspect of the Seaglider may be the speed at which it can travel (approximately 25 cm/s), and subsequently the inability to keep a steady course while crossing a current with a strong depth-averaged velocity. The pilots can combat this to a certain extent and compensate by directing dives into the current. As discussed by (Høydalsvik et al., 2013), the Seaglider did not perform well in the NwASC for this exact reason. The strong barotropic current in the eastern branch makes a Seaglider survey of the entire NwAC difficult, but it complements the already established current meter moorings that monitor the NwASC. Used in combination, they can monitor the entire Atlantic Inflow in the Svinøy section. As the Seaglider is relatively slow, a full transect in a section as extensive as the Svinøy section can require longer than a month to complete (See transect details in table 3.3). However, a crossing of the NwAFC

requires only a few days and could be considered quasi-synoptic.

Perhaps the greatest advantage of the Seaglider, certainly with respects to current and transport estimates, is the depth-averaged current which is very useful for estimating the absolute geostrophic flow. While previous studies of the velocity in the Svinøy section have relied on the assumption of a reference level of no motion (Orvik et al., 2001; Mork and Blindheim, 2000). The depth-averaged current estimates allow us to set a level of "known" motion instead.

Our transport estimates which span a period of 7 months, revealed that the barotropic component of the transport accounts for more than half of the total transport of AW (Water with salinity greater than 35) in the western branch of the Svinøy section. Our results corroborate the findings by Høydalsvik et al. (2013) who also estimated a barotropic contribution exceeding half that of the total transport. This demonstrates that in an area such as the Svinøy section, the ability to calculate absolute geostrophic velocity is important in producing accurate transport estimates, as the deep flow is substantial. Our transport estimates, though comparable with other estimates from the Svinøy section, are relatively low. Whether we consider the baroclinic component of the transport only (Orvik et al., 2001; Mork and Skagseth, 2010), or total transport (Høydalsvik et al., 2013). However, in accordance with the results from Høydalsvik et al. (2013), our estimates are substantially higher than the average transport estimate based on dynamic topography from Mork and Skagseth (2010). Our comparison between the RCM-measured current at 1500 m depth and the estimated current at 1000 m depth shows an overall agreement, which indicates that our current and transport estimates are indeed reasonable.

We have demonstrated that stream-coordinate averaging is a useful method to produce an accurate rendition of a true temporal average of the NwAFC and the Polar Front in the Svinøy section compared to the usual method of Eularian averaging. The structure of the front and the resulting baroclinic jet which is usually observed in individual transects is retained to a great degree in comparison to the Eularian averaging which due to the quite vigorous meandering of the NwAFC has resulted in a smudged image of the front and the associated current. When studying a feature like the NwAFC and the Polar Front, which despite of its unstable nature is typically easily identified, the stream-coordinate averaging is applicable in producing realistic current profiles. However, studying a similar feature which isn't always as discernible or harder to pinpoint with accuracy, would likely produce less accurate results. Additionally, for lower resolution, like that of a traditional survey using a shipmounted CTD, the method would not be so suitable.

References

Aagaard, K., J.H. Swift, and E.C. Carmack. Thermohaline circulation in the Arctic Mediterranean Seas. *J. Geophys. Res.*, 90(C3):4833–4846, 1985. ISSN 2156-2202.

Bower, A.S. and N.G. Hogg. Structure of the Gulf Stream and Its Recirculations at 55°W. *J. Phys. Oceanogr.*, 26(6):1002–1022, June 1996. ISSN 0022-3670.

Brown, E., A. Colling, D. Park, J. Phillips, D. Rothery, and J. Wright. *Ocean circulation*. Butterworth-Heinemann, 2nd edition, 2001.

Cushman-Roisin, B. and J.-M. Beckers. *Introduction to geophysical fluid dynamics physical and numerical aspects*, volume 101 of *International geophysics series*. Academic Press, 2nd edition, 2011.

Eriksen, C.C., T.J. Osse, R.D. Light, T. Wen, T.W. Lehman, P.L. Sabin, J.W. Ballard, and A.M. Chiodi. Seaglider: a long-range autonomous underwater vehicle for oceanographic research. *Oceanic Engineering, IEEE Journal of*, 26(4):424–436, Oct 2001. ISSN 0364-9059.

Halkin, D. and T. Rossby. The Structure and Transport of the Gulf Stream at 73°W. *Journal of Physical Oceanography*, 15:1439–1452, 1985.

Høydalsvik, F., C. Mauritzen, K.A. Orvik, J.H. LaCasce, C.M. Lee, and J. Gobat. Transport estimates of the Western Branch of the Norwegian Atlantic Current from glider surveys. *Deep Sea Research Part I: Oceanographic Research Papers*, 79(0): 86–95, 2013. ISSN 0967-0637.

iRobot 1KA Seaglider User's Guide. iRobot corporation, 2012.

Janzen, C.D. and E.L. Creed. Physical oceanographic data from Seaglider trials in stratified coastal waters using a new pumped payload CTD. In *OCEANS 2011*, pages 1–7, Sept 2011.

Johns, W.E., T.J. Shay, J.M. Bane, and D.R. Watts. Gulf Stream structure, transport, and recirculation near 68°W. *J. Geophys. Res.*, 100(C1):817–838, 1995. ISSN 2156-2202.

Mauritzen, C., E. Hansen, M. Andersson, B. Berx, A. Beszczynska-Möller, I. Burud, K.H. Christensen, J. Debernard, L. Steurde , P. Dodd, S. Gerland, Ø. Godøy, B. Hansen, S. Hudson, F. Høydalsvik, R. Ingvaldsen, P.E. Isachsen, Y. Kasajima, I. Koszalka, K.M. Kovacs, M. Køltzow, J. LaCasce, C.M. Lee, T. Lavergne, C. Lydersen, M. Nicolaus, F. Nilsen, O.A. Nøst, K.A. Orvik, M. Reigstad, H. Schyberg, L. Seuthe, Ø. Skagseth, J. Skarðhamar, R. Skogseth, A. Sperrevik, C. Svensen, H. Søiland, S.H. Teigen, V. Tverberg, and C. Wexels Riser. Closing the loop - approaches to monitoring the state of the arctic mediterranean during the international polar year 2007 - 2008. *Progress in Oceanography*, 90:62–89, 2011. ISSN 0079-6611.

Mork, K. A. and Ø. Skagseth. A quantitative description of the Norwegian Atlantic Current by combining altimetry and hydrography. *Ocean Science*, 6(4):901–911, 2010.

Mork, K.A. and J. Blindheim. Variations in the Atlantic inflow to the Nordic Seas, 1955-1996. *Deep Sea Research Part I: Oceanographic Research Papers*, 47(6):1035–1057, 2000. ISSN 0967-0637.

Mork, M. Circulation Phenomena and Frontal Dynamics of the Norwegian Coastal Current. *Philosophical Transactions of the Royal Society of London. Series A, Mathematical and Physical Sciences*, 302(1472):635–647, 1981. ISSN 00804614.

National Geophysical Data Center, NOAA U.S. Department of Commerce, NESDIS. TerrainBase, Global 5 Arc-minute Ocean Depth and Land Elevation from the US National Geophysical Data Center (NGDC), 1995. URL http://rda.ucar.edu/datasets/ds759.2/.

Nøst, O.A. and P.E. Isachsen. The large-scale time-mean ocean circulation in the Nordic Seas and Arctic Ocean estimated from simplified dynamics. *Journal of Marine Research*, 61(2):175–210, 2003.

Orvik, K. A. and P. Niiler. Major pathways of Atlantic water in the northern North Atlantic and Nordic Seas toward Arctic. *Geophysical Research Letters*, 29(19):21–24, 2002. ISSN 1944-8007.

Orvik, K. A., Ø. Skagseth, and M. Mork. Atlantic inflow to the Nordic Seas: current structure and volume fluxes from moored current meters, VM-ADCP and SeaSoar-CTD observations, 1995 - 1999 . *Deep Sea Research Part I: Oceanographic Research Papers*, 48(4):937–957, 2001. ISSN 0967-0637.

Orvik, K.A. and Ø. Skagseth. The impact of the wind stress curl in the North Atlantic on the Atlantic inflow to the Norwegian Sea toward the Arctic. *Geophysical Research Letters*, 30(17):n/a–n/a, 2003. ISSN 1944-8007.

Orvik, K.A., P.M. Haugan, K. Kvalsund, I. Hessevik, and E.M. Bruvik. The Norwegian Atlantic Current Observatory (NACO). In *ICES Annual Science Conference*, 2013.

Østerhus, S., W.R. Turrell, S. Jónsson, and B. Hansen. Measured volume, heat, and salt fluxes from the Atlantic to the Arctic Mediterranean. *Geophysical Research Letters*, 32(7):n/a–n/a, 2005.

Poulain, P.-M., A. Warn-Varnas, and P.P. Niiler. Near-surface circulation of the Nordic seas as measured by Lagrangian drifters. *Journal of Geophysical Research: Oceans*, 101(C8):18237–18258, 1996. ISSN 2156-2202.

Rossby, T., M.D. Prater, and H. Søiland. Pathways of inflow and dispersion of warm waters in the Nordic seas. *Journal of Geophysical Research: Oceans*, 114(C4):n/a–n/a, 2009. ISSN 2156-2202.

Rudnick, D.L., R.E. Davis, C.C. Eriksen, D.M. Fratantoni, and M.J. Perry. Underwater gliders for ocean research. *Marine Technology Society Journal*, 38:73–84, 2004.

Sætre, R. and R. Ljøen. *Proceedings the first international conference on port and ocean engineering under Arctic conditions, Trondheim, Norway Aug. 23-30, 1971*, chapter The Norwegian coastal current, pages 514 – 535. The Technical University of Norway, 1972.

Stull, R.B. *Meteorology for Scientisists and Engineers*. Cengage Learning, 2nd edition, 1999.

Voet, G., D. Quadfasel, K.A. Mork, and H. Søiland. The mid-depth circulation of the Nordic Seas derived from profiling float observations. *Tellus A*, 62(4):516–529, 2010. ISSN 1600-0870.

Wallace, John M. and P.V. Hobbs. *Atmospheric Science, an Introductory Survey*. Elsveir Academic Press, 2nd edition, 2006.